Flow and Kick

Koster, P.H.J.

P.H.J. Koster

Flow and Kick

Bachelor thesis

15 July 2022

Thesis supervisors: dr. F.W.J. Veerman
dr. Q. Peng

Leiden University
Mathematical Institute

Contents

1 Introduction

A dynamical system is an evolution rule that defines a trajectory as a function of a single parameter, time, on a set of states, the phase space [10]. In this thesis dynamical systems given by a system of differential equations are considered, see Chapter 2. Real-life dynamical systems can for instance describe population sizes of predator and prey species in an ecosystem, erosion of coastal defence areas, the average temperature of the world and financial markets. The liveliness, resilience and flexibility of all these developing, dynamical systems are tested continuously by sudden disruptions, which leads to the stretching and crossing of existing limits such that the characteristics of systems can be changed. Boundaries of systems are stretched or crossed by disturbances such as (over)fishing to fish populations [7], exorbitant greenhouse gas emission to global temperature, or maintenance activities like beach nourishment to coastal areas [6]. Sudden and instant disturbances may result in a significant change to the system, which are part of our interest. Even though the word "disturbance" normally has a negative connotation, disturbances can have positive effects. For instance the shooting of a part of a prey population in an ecosystem where their natural predator is absent so that animal suffering by starvation can be reduced to a minimum [13]..Repeated external changes, or to rephrase it in the language of dynamical systems, kicks that are applied repeatedly after a certain flow time, can influence the characterstics of stable states or balance unstable situations in the way we want, when the right change is applied at the right moment. Based on the theoretical framework of flow-kick systems which is developed in [11], this thesis will analyse specific disturbances by both numerical and theoretical analysis, by answering the main research question how flow-kick systems function. The main question is answered in four chapters by considering the following subquestions in detail:

1. How do flow-kick disturbances function in one-dimensional dynamical systems?
2. In what way do higher-dimensional flow-kick systems differ from one-dimensional ones?
3. How do flow-kick and flow-push systems relate to each other?
4. In what way can fast-slow and flow-kick systems be linked and how do instant disturbances function in fast-slow systems?

The scientific context on which the following chapters and previous questions are based, encloses the research done by Mary Lou Zeeman et al. in [11]. The article introduces a flow-kick framework that quantifies resilience to disturbances explicitly in term of their magnitude and frequency. Chapter 2 portrays this theoretical framework together with some basic concepts of dynamical systems. By elaborating on examples about ecosystems and climate systems the article illustrates the potential complexity of flow-kick dynamics and in its appendix mathematical arguments that establish the basis for their observations are presented. Since some assumptions are made, the first proposition proved in the article directly raises the first subquestion. In the proposition is stated which points belong to the resilience boundary that divide the stable from unstable disturbances defined by a pair consisting of flow time τ and a kick κ for a one-dimensional vector field with only one local minimum on a certain interval. However, in real-life examples these dynamics describe a very specific case. Therefore, we would like to know what occurs with the one-dimensional flow-kick dynamics if the vector field generating the flow in the undisturbed system has several local minima on (a, b). This question will be treated in Chapter 3 and will bring us closer to answering the first subquestion. Furthermore, it would be unrealistic to fix the disturbance for all of eternity. Interventions that change the kick size based on done observations are not uncommon and therefore, we also consider the influence of this time-dependency in Chapter 3.

The flow-kick framework is combined with theory on dynamical systems including the Hartman-Grobman theorem [10]. The Hartman-Grobman theorem which will come in handy when analyzing n-dimensional dynamical systems with $n \geq 2$. In one-dimensional systems the only choice we can make relating to the kick is the time the system has to recover from the instant change. In n-dimensional systems, however, the direction of the kick might also have tremendous impact on the stability and possible periodicity of orbits. As a result, we are interested in to what extent the direction and the magnitude of the kick influences the flow-kick dynamics. Besides this, we attempt to obtain periodic flow-kick orbits for unstable equilibria. In contrast with the real-life examples from [11] and the difficulties one encounters when considering unstable equilibria in these systems, we leave the concrete examples behind in Chapter 4. This way, new and more abstract options are opened up. This leads to an extended notion of recovering and we ask ourselves what it exactly means to recover from a disturbance in a higher-dimensional system to be able to answer the second subquestion.

Sometimes the duration of a kick is not negligible to the length of the processes described in the underlying dynamics. In stead of kicks, one has a push in the system. A lake can for example be polluted for a couple of years by a factory that leaks (degradable) chemicals. When the chemicals are easily degraded, the time the pollution took place is not negligible in proportion to the time it takes for the system to recover from the pollution [14]. Another example of pushes are wildfires or heathland fires. These heathland fires, however, can be considered like an intrinsic property of the system, since some heathlands need these fires regularly to flourish [12]. In the previous examples, the change is not instant, and therefore, the disturbances can better be described as pushes with a certain duration than as kicks that take zero time. This flow-push system raises up the research question whether there is a substantial difference between the flow-kick and flow-push dynamics.

To embroider on the notion that heathland fires can also be approached as an intrinsic part of the dynamical system describing them, fast-slow systems are singled out. In comparison to flow-kick or -push dynamics, the fast-slow systems enclose sudden changes in their definition, because the state variables function on different time scales. Accordingly, fast-slow systems are defined and an example, the Saltzman-Maasch climate model, is considered. Since we want to know how fast-slow and flow-kick systems can be linked and how kicks function in fast-slow dynamics, Chapter 6 zooms in on this subject.

The structure of the different chapters are similar, except for Chapter 2. Since Chapter 2 mainly states known theory, less examples are included than in Chapter 3 until 6. The chapters on flow-kick dynamics in one- and higher-dimensional systems, Chapter 3 and 4, first approach the subject theoretically and then numerically. This method persists roughly in Chapter 5 and 6. The final chapter will include a conclusion of the findings and answer the research questions.

2 Defining flow-kick dynamics

Kicks are instantaneous large perturbations that are applied to an undisturbed dynamical system. To construct a theoretical framework of flow-kick dynamics, we therefore first need to define these systems. Throughout this thesis, we assume that for $x \in \mathbb{R}^n$ the undisturbed dynamics are determined by a system of ordinary differential equations

$$\dot{x} = \frac{dx}{dt} = f(x). \tag{2.1}$$

From now on, we assume that $f : \mathbb{R}^n \to \mathbb{R}^n$ is sufficiently smooth, so $f \in C^k$ for some $k \geq 1$. After applying a kick κ, the system is given a certain time during which again only the undisturbed system determines the flow. This time is called the recovery time or flow time, τ, and is, just as kick κ, an intrinsic part of the flow-kick map $G : \mathbb{R}^n \to \mathbb{R}^n$ defined by

$$G_{\tau,\kappa}(x) = \phi_\tau(x) + \kappa. \tag{2.2}$$

Here, $\phi_\tau(x) : \mathbb{R}^n \to \mathbb{R}^n$ is the flow generated by the vector field f from (2.1). Basic properties of flow ensure that $\phi_0(x) = x$ for all $x \in \mathbb{R}^n$ and that, for all $s \in \mathbb{R}$, flowing for time $s + t$ is the same as first flowing for time s and then t, so $(\phi_t \circ \phi_s)(x) = \phi_t(\phi_s(x)) = \phi_{s+t}(x)$ [10]. To analyse the resilience of a system to these flow-kick disturbances, we first focus on the basin of attraction of equilibrium point x_*. Since x_* is an equilibrium it holds that $f(x_*) = 0$.

Definition 2.1. *An equilibrium x_* of flow ϕ_t is stable if for any neighborhood N of x^* there exists a neighborhood $M \subseteq N$ such that for $\phi_t(x) \in N$ for all $t \geq 0$ if $x \in M$. Furthermore, if $\lim_{t\to\infty} d(\phi_t(x), x_*)$, with $d : \mathbb{R}^n \times \mathbb{R}^n \to \mathbb{R}$ the Euclidean distance between the points, then x_* is asymptotically stable (see Figure 2.1).*

The stability and character of x_* can be determined by finding the linearization of (2.1) around x_*, which is given by $Df : \mathbb{R}^n \to \mathbb{R}^n$ that is

$$Df(x) = \begin{pmatrix} \frac{\partial f}{\partial x_1} & \dots & \frac{\partial f}{\partial x_n} \end{pmatrix}. \tag{2.3}$$

By evaluating Df in x_* the eigenvalues $\lambda_1, \dots, \lambda_n$ of $Df(x_*)$ can be obtained. Assume that x_* is a hyperbolic equilibrium, then for all $i \in \{1, \dots, n\}$ we have $Re(\lambda_i) \neq 0$ [10]. For hyperbolic equilibria the approach used for determining stability and character of equilibria is based on the following theorem.

Theorem 2.1 (Hartman-Grobman Theorem [10])**.** *Let x_* be a hyperbolic equilibrium of a C^1 vector field f with associated flow ϕ_t, then there exists a neighborhood N of x_* such that ϕ is topologically conjugate to its linearization Df on N. In other words, there exists a homeomorphism $h : \mathbb{R}^n \to \mathbb{R}^n$ such that $Df = h^{-1} \circ f \circ h$.*

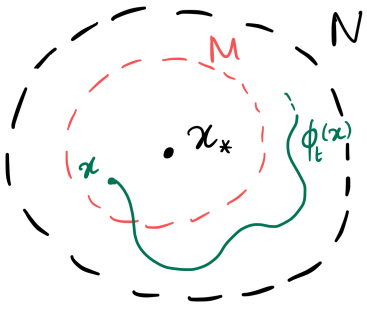

Figure 2.1: A neighborhood N of stable equilibrium x_* such that there is a neighborhood $M \subseteq N$ such that flow $\phi_t(x)$ will stay inside N for all $t \geq 0$ if $x \in M$.

A sketch of the proof of Theorem 2.1 can be found in [10]. Being able to translate properties of linear systems into a nonlinear context is a very convenient tool while studying equilibria of nonlinear systems. The stability of equilibria in linear systems is determined by their eigenvalues, which we can obtained quite easily. In the two-dimensional linear systems this leads to following ways to characterize the equilibria.

First we assume that both imaginary parts of the eigenvalues are zero, $Im(\lambda_1) = Im(\lambda_2) = 0$. Now, the real parts of the eigenvalues and the number of distinct eigenvectors determine the character of the equilibrium. The equilibrium is an asymptotically stable node for two distinct eigenvalues with $Re(\lambda_2) < Re(\lambda_1) < 0$ for coinciding eigenvectors, see "stable node (iii)" in Figure 2.2 and for two distinct eigenvectors (ii). For coinciding eigenvalues with $Re(\lambda_1) = Re(\lambda_2) < 0$ and two distinct eigenvectors, the equilibrium is also a stable node (i). When $Re(\lambda_2) \geq Re(\lambda_1) > 0$ the equilibria are nodes as well, but then the direction of the orbits in Figure 2.2 is reversed and the nodes are unstable. An equilibrium is an unstable saddle point when $Re(\lambda_1) < 0 < Re(\lambda_2)$.

If the imaginary parts, however, are nonzero, write $\lambda_1 = \alpha + i\beta, \lambda_2 = \alpha - i\beta$, with α and $\beta \in \mathbb{R}$, we have a stable center point for $\alpha = 0$, an asymptotically stable focus for $\alpha < 0$ or an unstable focus for $\alpha > 0$. These characters are also depicted in Figure 2.2 [1].

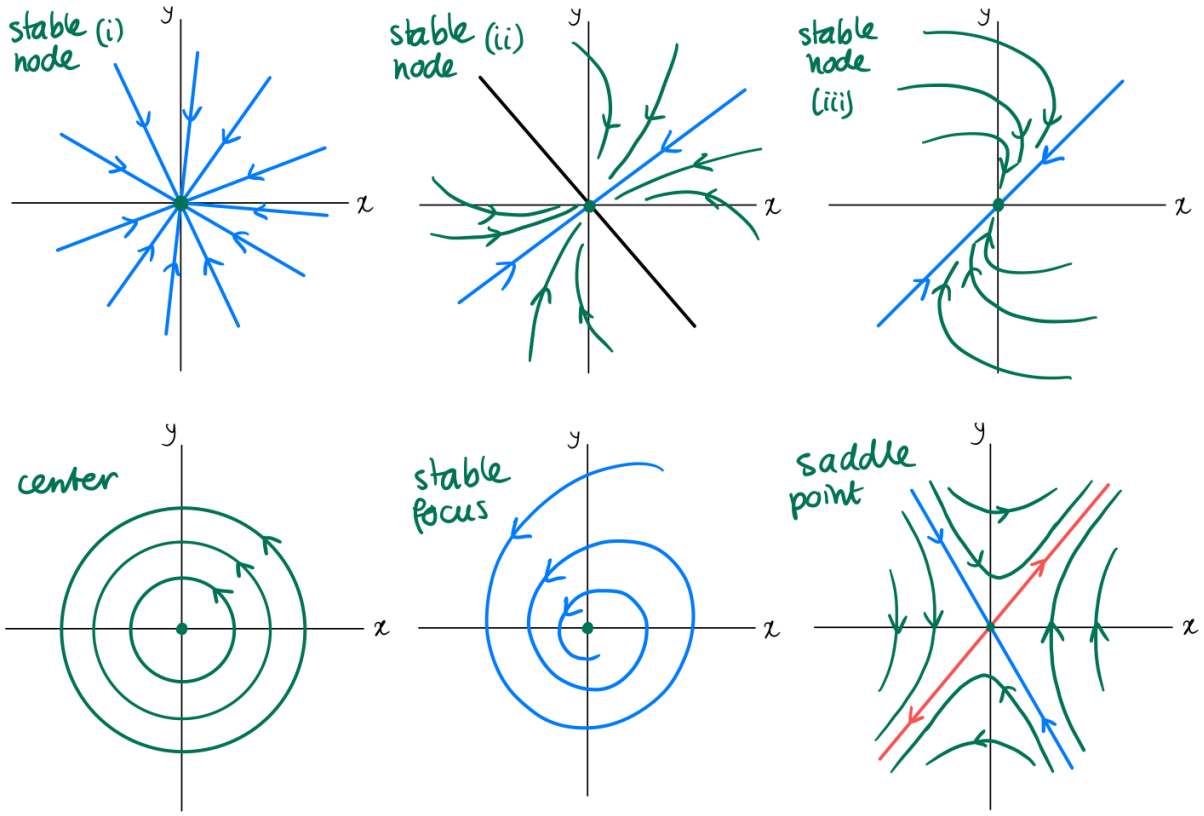

Figure 2.2: Characters of stable equilibria and a saddle point equilibrium. Unstable versions are exactly the same, except for the direction of the arrows, this direction is reversed.

This thesis, except for a part of Chapter 4, focuses on asymptotically stable equilibria and their basin of attraction in relation to flow-kick maps.

Definition 2.2. *The basin of attraction (or stable set) of an invariant set, Λ, is the set of all points $x \in \mathbb{R}^n$ for which $\lim_{t\to\infty} d(\phi_t(x), \Lambda) = 0$.*

Note that singletons consisting of an equilibrium are by definition invariant sets and thus have a basin of attraction that contains at least the equilibrium. This notion is needed to

introduce the concept of stability for flow-kick systems.

Definition 2.3. *A disturbance (τ, κ) is stable if the flow-kick trajectory of point $x \in \mathbb{R}^n$ stays in the basin of attraction of equilibrium x_*, $\mathcal{B}(x_*)$, for all $t > 0$.*

Definition 2.3 follows from [11] and seems quite strict, since the trajectory needs to be in $\mathcal{B}(x_*)$ for all $t > 0$. Note, however, that if there would exist a $T > 0$ such that the flow-kick trajectory would not be in $\mathcal{B}(x_*)$, the undisturbed system would not be able to recover from the disturbance and therefore never return to the basin of attraction, thus be unstable. Besides this, the flow-kick trajectory of the disturbance is initiated at x_* and x_* is contained in its own basin of attraction. Thus, the flow-kick trajectory of x_* should stay in the basin of attraction for all $t > 0$.

In Figure 2.3 the basin of attraction of asymptotically stable equilibrium x_*, $\mathcal{B}(x_*) = (A, \infty)$, is highlighted in red. The associated system is given by

$$\dot{x} = f(x) = rx\left(\frac{x}{A} - 1\right)\left(1 - \frac{x}{C}\right)$$

and describes the population growth in an ecosystem with carrying capacity $C = x_*$, and an Allee threshold, A [5]. The coefficient r is the intrinsic growth rate of the population. This Allee threshold is an unstable equilibrium and denotes a critical population size. If the population size, x, is smaller than A, it will decrease such that the population collapses. If $x \in \mathcal{B}(a)$ this does not happen naturally, since x_* is an asymptotically stable equilibrium in the undisturbed dynamics. A substantial kick can, however, make the population size fall below the threshold. Figure 2.3 depicts a stable kick κ in blue and the orbits during the flow time in green. The flow-kick trajectory of starting point x_* stays in its basin of attraction, in this case the time in which the system could to recover from κ was sufficient. If either the kick had been larger or the flow time shorter, this might not have been the case. In Section 3.1 we will return to this concept and make this observation precise.

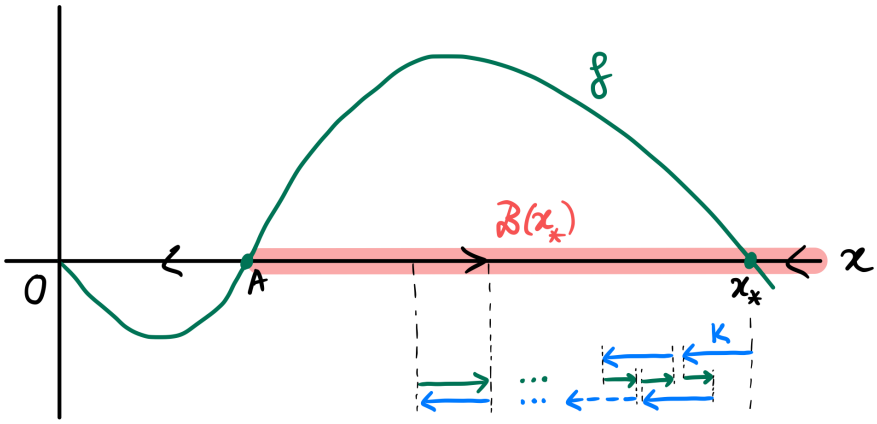

***Figure 2.3:** A one-dimensinal flow-kick system that describes population growth by $f(x) = rx\left(\frac{x}{A} - 1\right)\left(1 - \frac{x}{C}\right)$ with carrying capacity C, Allee threshold A such that $0 < A < C$, and r a constant for the intrinsic growth rate. Disturbances consist of a blue arrow for the kick and a green arrow indicating the flow during the flow time.*

3 One-dimensional flow-kick systems

For the convenience of analysing one-dimensional flow-kick systems, we assume without loss of generality that the vector field can be divided into intervals such that it is similar to the f in Figure 3.1 on these intervals. This means that the system $\dot{x} = f(x)$ has an asymptotically stable equilibrium, a, and an unstable one, b. We can assume that $f(x) < 0$ on (a, b), that the derivative of f in a is negative, $f'(a) < 0$, and that this derivative is positive in b, $f'(b) > 0$. At a first glance, f describing the population growth (see Figure 2.3) does not meet these requirements on the interval $(A - \varepsilon, x_* + \varepsilon)$, with $0 < \varepsilon \ll d(\tilde{x}, A)$ and $\tilde{x} \in (0, A)$ such that $f'(\tilde{x}) = 0$. Mirroring f on this interval solves our problem. After rotating, x_* is the left and asymptotically stable equilibrium, A the right and unstable one, and are the function values also smaller than zero in between both equilibria. All the reasoning on the one-dimensional systems can via this way be reformulated. In this case, interesting things only happen when $\kappa > 0$. For $\kappa < 0$ and all $\tau > 0$ the flow-kick trajectory of a will stay inside its basin of attraction. For $\kappa > 0$ it is, however, possible to leave $\mathcal{B}(a)$.

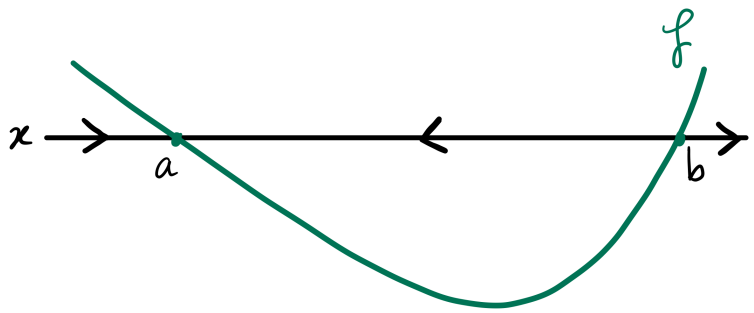

Figure 3.1: A one-dimensional system generated by f ***with two equilibria*** a ***and*** b ***such that*** $f(x) < 0$ ***for*** $x \in (a, b)$ ***and*** $f'(a) < 0, f'(b) > 0$***.***

3.1 Resilience boundaries

The stability of a flow-kick trajectory depends on the pair (τ, κ) for which flow-kick map $G_{\tau,\kappa}$ is defined. All the disturbances (τ, κ) to which the system is resilient together, form the resilient region, R^s, of the (τ, κ)-space or disturbance space. The disturbance space is given by $\mathbb{R}_{>0} \times \mathbb{R}_{>0}$ and since a disturbance is either stable or unstable, the disturbances in $R^u := \mathbb{R}_{>0} \times \mathbb{R}_{>0} \setminus R^s$ form the non-resilient region. For these disturbances the flow-kick trajectory of equilibrium x_* escapes from $\mathcal{B}(x_*)$. Since f is sufficiently smooth, this results in a sharp separation between these regions. In [11] a new metric to quantify the resilience of (eco)systems, with the so-called resilience boundary, R, at its core, is defined on the disturbance space.

Definition 3.1. *The resilience boundary, R, for the basin of attraction of a, $\mathcal{B}(a)$, separates disturbance patterns (τ, κ) for which the flow-kick trajectory of a remains in $\mathcal{B}(a)$ from the disturbance patterns (τ, κ) for which the flow-kick trajectory of a escapes from $\mathcal{B}(a)$.*

Proposition 3.1. *If the function f has at most one maximum on (a, b), then R consists of exactly these disturbances (τ, κ) for which τ is the minimum time in which the system can recover by $-\kappa$, taken over all possible intervals of length $|\kappa|$ between a and b.*

A proof of Proposition 3.1 can be found in [11]. Note that Definition 3.1 only fixed disturbances for a as initial value of a solution of $\dot{x} = f(x)$ are considered, which means that the first kick κ is applied at a, after letting a flow forward for time τ. Since $f(a) = 0$, the kick starts in a itself. This does not cause trouble if the assumption is made that f has at

most one minimum on (a, b). Figure 3.2 depicts a resilience boundary for a flow that meets the assumptions from before.

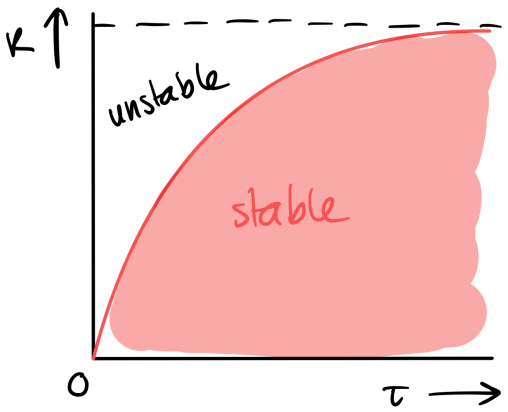

Figure 3.2: The (τ, κ)-space is separated in a non-resilient region with unstable disturbances and a resilient region with stable disturbances, separated by a resilience boundary (in red).

Allowing f to have more than one minimum on (a, b) has interesting consequences for Definition 3.1. Definition 3.2 is an extension of Definition 3.1.

Definition 3.2. *The resilience boundary for a point $x_0 \in \mathcal{B}(a)$, R_{x_0}, separates disturbance patterns (τ, κ) for which the flow-kick trajectory is initiated at x_0 remains in $\mathcal{B}(a)$ from disturbance patterns (τ, κ) for which this flow-kick trajectory escapes from $\mathcal{B}(a)$.*

Proposition 3.2. *Let $A : \mathcal{B}(a) \times \mathbb{R}_{>0} \to \mathbb{R}$ for all $x \in \mathcal{B}(a)$ and $\kappa > 0$ be given by $A(x, \kappa) = \tau$ such that τ is the minimal time in which the system can recover from $-\kappa$ taken over all possible intervals with length $|\kappa|$ between x and b. Now, the resilience boundary of x_0 is given by $\{A(x_0, \kappa) = \tau : \kappa > 0\}$. For $x_0 = a$, we find that $R = \{A(a, \kappa) = \tau : \kappa > 0\}$.*

Proof. The fact that a is asymptotically stable provides that for all $x \in \mathcal{B}(a)$ holds that $\lim_{t\to\infty} \phi_t(x) = a$. Thus, for all $\varepsilon > 0$ such that $\min_{y\in\partial\mathcal{B}(a)} d(a, y) > \varepsilon$, there exists a $T \geq 0$ such that $d(\phi_t(x), a) < \varepsilon$. Let $x(t)$ be the solution to the initial value problem $\dot{x} = f(x)$ with initial value $x(0) = x_0$ such that $d(x_0, a) = \varepsilon$ and assume, without loss of generality, that $x_0 > a$. Let kick κ with $0 < \kappa < d(x_0, a)$ be given and consider

$$\tau = F(k) = \int_{x_0-\kappa}^{x_0} \frac{1}{f(x)} dx, \tag{3.1}$$

this integral defines the minimal time it takes the system to recover from kick κ inside of $(a - \varepsilon, a + \varepsilon)$ and follows from separation of variables in (2.1). This ensures that there exists a τ in which the system can recover from $-\kappa$. This τ is, however, not per definition minimal. Minimizing (3.1) over all $x_0 \in \mathcal{B}(a)$ with their associated solutions, gives that A exists for all $x \in \mathcal{B}(a)$. Note however, that A is not well-defined for $\kappa > \min_{y\in\partial\mathcal{B}(a)} d(x_0, y)$ since (3.1) then diverges.

Hence, the resilience boundary of $x_0 \in B(a)$ is given by $\{A(x_0, \kappa) = \tau : \kappa > 0\}$. For $x_0 = a$ we can find the values of τ the same way as before and since R was defined as the resilience boundary of the asymptotically stable equilibrium, we find $R = \{A(a, \kappa) = \tau : \kappa \in \mathbb{R}_{>0}\}$. □

In the previous proof, the fact that f can have several extrema on the basin of attraction does not have great consequences. Definition 3.2 is closely related to the concept of *convergence intervals*. In the following section the mentioned consequences emerge.

3.2 Convergence intervals

For a stable disturbance (τ, κ) the flow-kick trajectory of a point x_0 remains in $\mathcal{B}(a)$. In particular, it stays around a certain interval when time continues. These convergence intervals come in handy during further analysis, especially when f has several extrema on (a, b) and the values at which flow-kick processes are initiated differ.

Definition 3.3. *Let $\mathcal{I}_i(x_0) = [x_i, x_i + \kappa]$ for $i \in \{1, \ldots, j\}$ be the intervals over which it takes the system (2.1), with initial condition x_0, flow time τ to recover from kick κ. For disturbance (τ, κ) we define the convergence interval, $\mathcal{I}(x_0)$ as the interval $\mathcal{I}_i$ for which the distance $d(x_0, x_i)$ is minimized.*

In Definition 3.3 only the intervals over which flow time τ occurs are considered. Since both a and b are assumed to be equilibria and f is sufficiently smooth, the number of these intervals is finite. We are interested in these $\mathcal{I}_i(x_0)$, since the flow-kick trajectory initiated at x_0 stays in a neighborhood that contains $\mathcal{I}(x_0)$ after some time $T \geq 0$. This claim is captured by Theorem 4.1 and proved for n-dimensional systems in Section 4.3. On the other hand, Definition 3.4 sheds a new light on the concept of convergence intervals.

Definition 3.4. *Let $\mathcal{I}_i(x_0) = [x_i, x_i + \kappa]$ for $i \in \mathbb{Z}_{\geq 0}$ be intervals the intervals on which the system (2.1) acts with initial condition x_i. For disturbance (τ, κ) we define the convergence interval, $\mathcal{I}(x_0)$ as the interval $\mathcal{I}_i$ with i the smallest index for which τ occurs over $\mathcal{I}_i$ and for which the distance $d(x_0, x_i)$ is minimized.*

Note that the x_i for which we consider the intervals $\mathcal{I}_i(x_0)$ are values at which a disturbance is applied to the system. Thus, the flow-kick trajectory of x_0 is by Definition 3.4 given by $\bigcup_{i \in \mathbb{Z}_{\geq 0}} \mathcal{I}_i(x_0)$. The times that occurs over $I_i(x_0)$ are not equal to τ, but converge to τ for $i \to \infty$. The convergence interval is therefore selected completely different from Definition 3.3, in Definition 3.3 τ occurs for all $\mathcal{I}_i(x_0)$ with $i \in \{1, \ldots, j\}$. Definition 3.4 can be useful when analyzing a flow-kick trajectory initiated at one point in-depth. However, this section looks at various initial values of the flow-kick map. From now on Definition 3.3 is used.

The fact that $\mathcal{I}(x_0)$ is selected from the $\mathcal{I}_i(x_0)$ by considering the distance between x_0 and x_i, makes us wonder what happens with the intervals for which (2.1) also can recover from kick κ in flow time τ. The following paragraphs will therefore divide the basin of attraction of a into intervals I_n, for which the flow-kick trajectory of initial value $\tilde{x}_0 \in I_n$ converges to $\mathcal{I}_i(\tilde{x}_0)$ for $i \in \{1, \ldots, j\}$.

Definition 3.5. *The basin of attraction of an asymptotically stable equilibrium can be divided into at least two initial condition intervals, I_r, with $r \geq 2$ such that for $x_0 \in I_{r_1}$ and $\tilde{x}_0 \in I_{r_2}$, with $r_1, r_2 \in \{1, \ldots, r\}$ holds for disturbance (τ, κ) that $\mathcal{I}(x_0) \neq \mathcal{I}(\tilde{x}_0)$.*

For all $i \in \{1, \ldots, j\}$ separations of variables yields the recovery time as a function of κ, for $\dot{x} = f(x)$ we obtain

$$\tau = F(\kappa) = \int_{x_i}^{x_i + \kappa} \frac{1}{f(x)} dx,$$

based on results from [11]. Figure 3.3 illustrates Definition 3.3 for a certain $f : \mathbb{R} \to \mathbb{R}$ with two local minima on (a, b). For a symmetric f with only one extremum we would now be able to find the resilience boundary, composed of points $(F(\kappa), \kappa)$, explicitly by solving and integrating for κ in terms of τ, since the shortest time in which the system can recover by $-k$ between a and b occurs over an interval of length κ centered on $(a + b)/2$ [11]. We, however, did not assume this and are obliged to use a different approach to analyse the system then using this symmetry and thus divide $\mathcal{B}(a)$ into I_r, with $r \in \{1, 2, 3\}$ for the example in Figure 3.3.

Assume that f has asymptotically stable equilibrium a and unstable equilibrium b with $a < b$ such that $f'(a) < 0$, $f'(b) > 0$ and that $f(x) < 0$ for all $x \in (a, b)$. Denote the local minima of f on (a, b) by m_i for all $i \in \{1, \ldots, n\}$, thus n is the number of local minima of f on (a, b). Label the local maxima by M_i with $i \in \{1, \ldots, N\}$. For now, we have $n = 2$. Consider $x_0 \in (a, m_1)$ such that there exists a stable disturbance (τ, κ) for x_0 and fix this pair (τ, κ). We have that

$$\tau = \int_{\mathcal{I}(x_0)} \frac{1}{f(x)} dx$$

with $\mathcal{I}(x_0)$ the convergence interval of x_0 minimizing the distance between x_0 and the left boundary, α_1, of $\mathcal{I}(x_0)$. So, $\mathcal{I}(x_0) = \mathcal{I}_1(x_0)$. Define the interval I_1 by (a, α_1).

By Definition 3.3, $\mathcal{I}(x_0)$ minimizes $d(x_0, \alpha_1)$ in order that τ occurs over $\mathcal{I}(x_0)$. It can however be the case that $\mathcal{I}(x_0)$ is not the only interval over which the system can recover in τ by $-\kappa$. In Figure 3.3 the flow time also occurs over $\mathcal{I}_2(x_0)$ and $\mathcal{I}_3(x_0)$. Assume, in general, that there exists an $i \in \{1, \ldots, j\}$ such that $\mathcal{I}_i(x_0) \neq \mathcal{I}(x_0)$ and that τ occurs over this interval. Mark that $\mathcal{I}_i \subseteq I_2 = (\alpha_1, \alpha_2)$ and choose α_2 such that the time to recover from kick κ on $(\alpha_2, \alpha_2 + \kappa)$ is minimized on (M_1, M_2). However, since $n = 2$ we have in this case that $r = 3$. (The value of r depends on the value of f in the extrema.) Therefore, the found α_2 is not the value of α_2 we were looking for, if $r > 4$ it would have been. As $f \in C^1$ there is a $\tilde{\alpha}_2 \in (m_2, b)$ such that

$$\tau = \int_{\tilde{\alpha}_2}^{\tilde{\alpha}_2 + \kappa} \frac{1}{f(x)} dx.$$

Note that $\tilde{\alpha}_2$ is the left boundary of $\mathcal{I}_3(x_0)$. We have $I_2 = (\alpha_1, \tilde{\alpha}_2)$. The orange interval is the interval over which the minimal time for which the system can recover from $-\kappa$ occurs and shows therefore, that τ is not the minimal time for which the flow-kick trajectory initiated at $\tilde{x}_0$ is stable and thus $\tilde{\alpha}_2$ exists. For all initial values $\tilde{\tilde{x}}_0 \in (\tilde{\alpha}_2, b)$ is the flow-kick trajectory of disturbance (τ, κ) unstable.

The flow-kick system will find itself in different stable states depending on the position where the instant disturbances were first applied, in Figure 3.3 all flow-kick trajectories for disturbance (τ, κ) starting in I_1, $x_0 \in I_1$ converge to $\mathcal{I}_1(x_0)$, all trajectories initiated in I_2 converge to $\mathcal{I}_2(x_0)$ and all flow-kick orbits that start in $\{x : x \in (a, b)\} \setminus \{x : x \in I_1 \cup I_2\}$ are unstable.

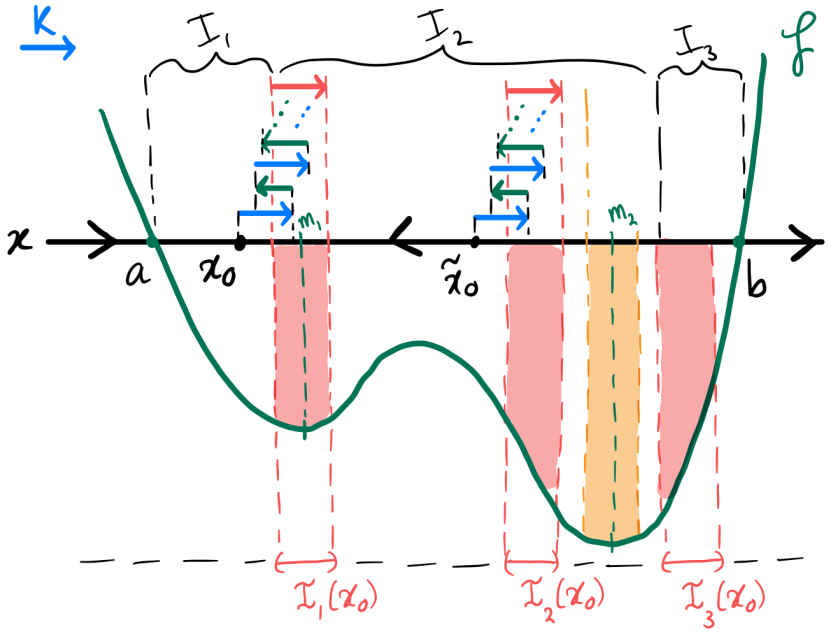

***Figure 3.3:** If f has more than one extremum on (a, b) it can be possible that the flow-kick trajectory defined by a fixed disturbance (τ, κ) of distinct initial values converges to separate convergence intervals.*

3.3 Kicks depending on time

The disturbances considered in the previous sections do not depend on how much time has already passed. Based on real-life examples such as the effect of the fishing industry on the fish population size in an (eco)system this assumption is, in spite its convenience, not realistic. Both the frequency and the size of kicks could namely change in the course of time, particularly when looking at disturbances caused by independent actors such as humans. If factors or real-life observations would indicate that a disturbance (τ, κ) is unstable and will eventually lead to the collapse of a population, as the flow-kick trajectory gets below the Allee threshold, one could decide to decrease the kick size after some moment in time. By letting the kick or the flow time depend on time, we can interfere with the flow-kick dynamics and possibly change a disastrous outcome into an alternative. The time dependency of a disturbance can, of course, be defined in quite exotic ways, however, for now we only consider the following time dependency.

Proposition 3.3. *Assume that (τ, κ) is an unstable disturbance for $x_0 \in (a, b)$ for vector field f such that $|\kappa| < b - x_0$, so there exists a $T \in \mathbb{R}_{>0}$ for which the flow-kick trajectory of x_0 is in $\mathcal{B}(a)$. Then there exists a stable disturbance $(\tau, K(t))$ with*

$$K(t) = \begin{cases} \kappa & \text{for } 0 \leq t < T \\ \kappa_T & \text{for } t \geq T \end{cases},$$

with κ_T smaller or equal to the kick $\kappa_{\max}$ for which the value of the flow-kick trajectory of x_0 after time T, $G_T(x_0)$, can still recover from $-|\kappa_{\max}|$ in recovery time τ.

Proof. After time T, the flow-kick map $G_{\tau,\kappa}$, see (2.2), has been applied $(T - T \mod \tau)$ times, after the disturbance has been applied for the $(T - T \mod \tau)$-th time, $G_{\tau,\kappa}^{(T-T \mod \tau)}(x_0)$, flows forward for $T \mod \tau$. Thus, $G_T(x_0) = \phi_{(T \mod \tau)}\left(G_{\tau,\kappa}^{(T-T \mod \tau)}(x_0)\right)$. Consider the resilience boundary for the point $G_T(x_0)$, $R_{G_T(x_0)}$. By means of Proposition 3.1 we can find a κ_T such that the flow-kick trajectory of $G_T(x_0)$ stays in basin of attraction $\mathcal{B}(a)$. □

3.4 Numerical results

Flow-kick dynamics were implemented in one-, two- and three-dimensional systems in the Python code that can be found in Appendix A. Here we will focus on the one-dimensional implementation in `flowkick.py` from Appendix A.1. In Section 4.4 the two- and three-dimensional situations are portrayed. We use the (straight)forward Euler method to construct the solution of the dynamical system per coordinate and the desired disturbances (τ, κ) is applied to this undisturbed dynamics. For `N+1` and time `T` an array `t` is constructed using *numpy.linspace()*, between consecutive values in `t` are time steps with size `dt = T/N`. Based on the index of `t` and flow time τ, κ is applied by appending `xG[-1] + dt*f(xG[-1]) + k` to the array `xG`, which stores the values of the flow-kick map. In this case, `f` is the ordinary differential equation that describes the undisturbed dynamics.

3.4.1 Influence of kick frequency and size in one-dimensional flow-kick systems

The Figures 3.4 and 3.5 both depict two flow-kick trajectories for initial value $x_0 = 75$ for an Allee population model defined by

$$f(x) = rx\left(\frac{x}{A} - 1\right)\left(1 - \frac{x}{C}\right), \tag{3.2}$$

with $r = 0.5$, $A = 50$ and $C = 200$. The disturbances characterizing the blue flow-kick trajectories are in the resilient region of the (τ, κ)-space and the disturbances defining the red trajectories are in the non-resilient region, since the population breaks down when the Allee threshold is exceeded. In Figure 3.4 two different disturbances (τ_1, κ_1) and (τ_2, κ_2) are considered. Kicks κ_1 and κ_2 have are the same for both trajectories, namely $\kappa_1 = \kappa_2 = -16$, but the flow times differ. The kick frequency of (τ_1, κ_1) is lower than the one of (τ_2, κ_2), we have $\tau_1 = 1.5\tau_2$ with $\tau_2 = 1$. For the higher kick frequency, so lower flow time the system has not enough time to recover from the kick, and therefore, the flow-kick trajectory x_0 for (τ_2, κ_2) is kicked below threshold $A = 50$ after $t = 7$.

Consider the disturbances in Figure 3.5, $(\tilde{\tau}_1, \tilde{\kappa}_1)$ is a stable disturbance in blue in contrast to unstable disturbance $(\tilde{\tau}_2, \tilde{\kappa}_2)$ in red. For the flow times holds that $\tilde{\tau}_1 = \tilde{\tau}_2$, on the other hand, the kicks have different sizes, $\tilde{\kappa}_1 = -15$ and $\tilde{\kappa}_2 = -16$. In short, modifying only the kick or the flow time of a disturbance can have great impact on the (in)stability of a flow-kick trajectory.

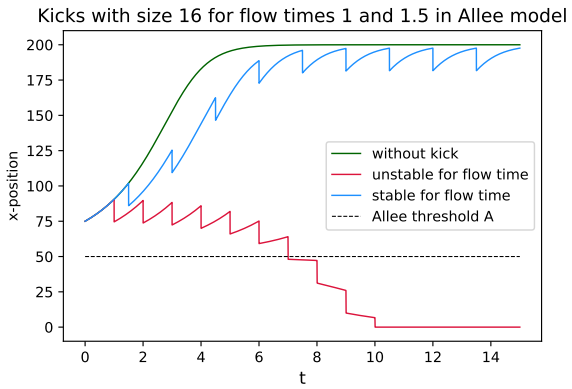

***Figure 3.4:** Two disturbances with different flow times, $\tau_1 = 1.5\tau_2$ with $\tau_2 = 1$, but same kick, $\kappa_1 = \kappa_2 = -16$.*

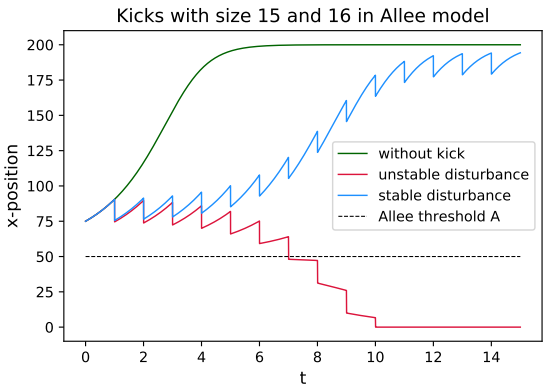

***Figure 3.5:** Two disturbances with different sizes, $\tilde{\kappa}_1 = -15$ and $\tilde{\kappa}_2 = -16$, but same flow time, $\tilde{\tau}_1 = \tilde{\tau}_2 = 1$.*

3.4.2 Convergence intervals

As described in Section 3.2 the convergence interval around which the flow-kick trajectory of fixed disturbance (τ, κ) remains, depends on the value at which the flow-kick trajectory is initiated. In Figure 3.6 this can be observed for a certain disturbance on the undisturbed system defined by

$$\dot{x} = f(x) = (x-2)^4 - 4(x-2)^2 - 2, \tag{3.3}$$

which is graphed in Figure 3.7. We have equilibria if $\dot{x} = 0$, thus $x_\pm = 2 \pm \sqrt{2+\sqrt{6}}$ are equilibria for(3.3). For fixed disturbance $(\tau, \kappa) = (0.042, 0.25)$ we can now find I_1, I_2 and I_3 from Definition 3.5 using *flowkick.py*, the Python code for one-dimensional systems can be found in Appendix A.1.

To start with I_1, we know that $I_1 \approx (a, \alpha_1)$ with a the asymptotically stable equilibrium x_-. The right boundary of I_1 is given by α_1 for which holds that

$$\tau = \int_{\alpha_1}^{\alpha_1+\kappa} \frac{dx}{f(x)} = \int_{\alpha_1}^{\alpha_1+\kappa} \frac{1}{(x-2)^4 - 4(x-2)^2 - 2} dx. \tag{3.4}$$

We find $\alpha_1 \approx 0.4381$ numerically, thus $I_1 \approx (x_-, 0.4381)$, and $d(\alpha_1, a)$ is minimized for $\alpha_1 \in \mathcal{B}(a)$. Note that, $[\alpha_1, \alpha_1 + \kappa] = \mathcal{I}(a)$. The second interval of initial conditions, I_2, such that the flow-kick trajectory converges to a different convergence interval than $\mathcal{I}_1 \approx (0.4381, 0.6881)$, is given by $I_2 = (\alpha_1, \tilde{\alpha}_2) \supseteq \mathcal{I}_1$ such that for $\tilde{\alpha}_2$ holds

$$\tau = \int_{\tilde{\alpha}_2}^{\tilde{\alpha}_2+\kappa} \frac{dx}{f(x)} = \int_{\tilde{\alpha}_2}^{\tilde{\alpha}_2+\kappa} \frac{1}{(x-2)^4 - 4(x-2)^2 - 2} dx, \tag{3.5}$$

with $\tilde{\alpha}_2 \in (M_1, b)$. Consider (3.5), we find

$$\begin{aligned} \tau &= \left[-\arctan\left(\frac{x-2}{\sqrt{2+\sqrt{6}}}\right) + \arctan\left(\frac{x-2}{\sqrt{-2+\sqrt{6}}}\right) \right]_{\tilde{\alpha}_2}^{\tilde{\alpha}_2+\kappa} \\ &= -\arctan\left(\frac{(\tilde{\alpha}_2+\kappa)-2}{\sqrt{2+\sqrt{6}}}\right) + \arctan\left(\frac{(\tilde{\alpha}_2+\kappa)-2}{\sqrt{-2+\sqrt{6}}}\right) \\ &\quad - \left(\arctan\left(\frac{\tilde{\alpha}_2}{\sqrt{2+\sqrt{6}}}\right) + \arctan\left(\frac{\tilde{\alpha}_2-2}{\sqrt{-2+\sqrt{6}}}\right) \right) \end{aligned} . \tag{3.6}$$

Solving (3.6) numerically for $\tilde{\alpha}_2$ gives $\tilde{\alpha}_2 = 3.257...$ or $\tilde{\alpha}_2 = 3.311....$ The flow-kick trajectory defined by disturbance $(\tau, \kappa) = (0.042, 0.25)$ for $x_0 \in (3.257..., 3.311...)$ converges to $\mathcal{I}_i(x_0) = (3.257..., 3.507...)$. We get $I_2 = (0.483..., 3.257...)$ and $I_3 = (3.257..., x_+)$. In Table 3.1 the convergence intervals for two different initial values are included.

In summary, for all $\tilde{x}_0 \in I_1$ we see that the convergence intervals of $\mathcal{I}(\tilde{x}_0)$ for fixed disturbance (τ, κ) are the same. For $x_0 \in I_2$ the convergence intervals also match. For flow-kick trajectories initiated in I_3, the disturbance that was originally stable appears to be unstable. Basins of attraction of asymptotically stable equilibria in a one-dimensional system can therefore be divided into at least two sections for which a flow-kick trajectory initiated in the other section has different properties, dependent on the number of local minima and the magnitude of the the minima.

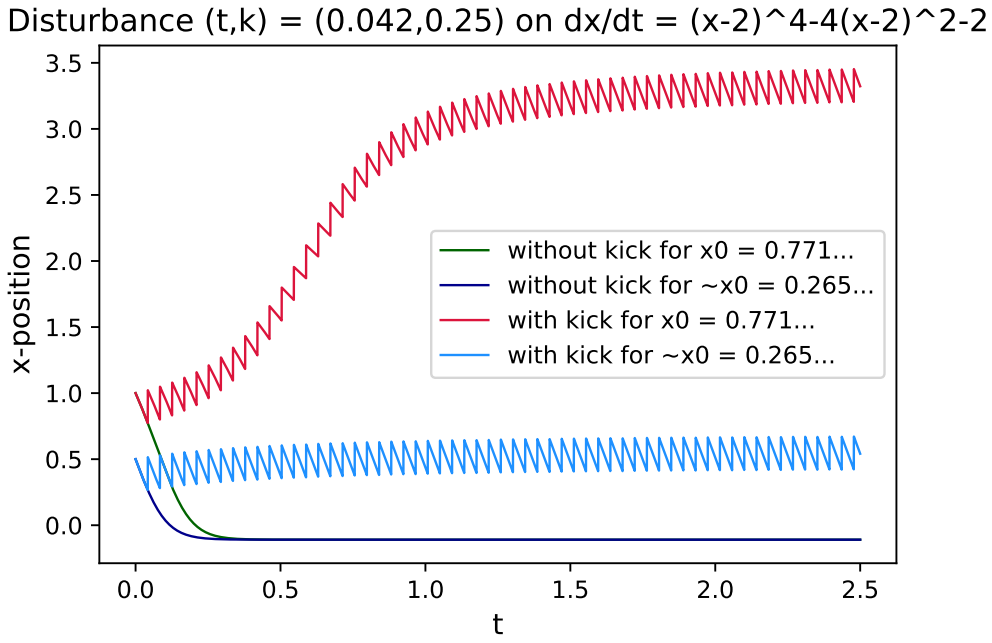

Figure 3.6: ***For distinct initial values,*** $x_0 = 0.771...$ ***and*** $\tilde{x}_0 = 0.265...$***, the stable disturbance*** $(\tau, \kappa) = (0.042, 0.25)$ ***has distinct convergence intervals.***

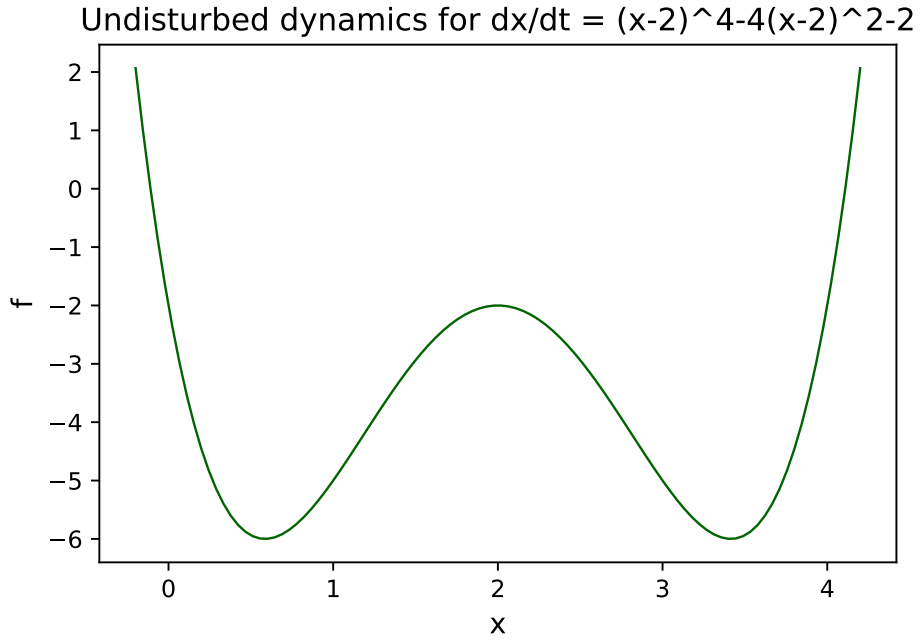

Figure 3.7: ***Undisturbed dynamics generated by vector field*** $f(x) = (x-2)^4 - 4(x-2) - 2$***. See Table 3.1 for the used input values.***

Initial value	Initial condition interval I_r	Convergence interval $\mathcal{I}$
$\tilde{x}_0 = 0.265...$	$I_2 = (0.483..., 3.257...)$	$(3.257..., 3.507...)$
$x_0 = 0.771...$	$I_1 = (x_-, 0.438...)$	$(0.438..., 0.688...)$

Table 3.1: ***Results for numerical analysis in Section 3.4.2 with disturbance*** $(\tau, \kappa) = (0.042, 0.25)$***.***

3.4.3 Time-dependent kicks

Practical examples of disturbances whose magnitude depends on time are population models that include an Allee threshold, a model with such a threshold is described by (3.2) and is already depicted in Figure 2.3 [7]. Both A and C are equilibria of this vector field, with $C = x_*$ is an asymptotically stable one.

Since f has only one mimimum on (A, x_*), the basin of attraction of x_* can be split up in two intervals, I_1 and I_2, constructed as in Section 3.2 and 3.4.2, for which the convergence intervals for fixed disturbance (τ, κ) differ. For all x_0 in interval $I_2 = (A, \alpha_1)$ the disturbances are unstable. In other words, for every $x_0 \in I_2$ there is a $T \geq 0$ such that $G_{\tau,\kappa}^{(T-T \mod \tau)}(x_0) \leq A$. Assuming that $T > 0$, with Proposition 3.3 we can define a stable disturbance $(\tau, K(t))$ based on the fixed disturbance (τ, κ) such that the system will still be able to recover from the kick, K describes in what way we intervene with the original kick dependent on time. This is illustrated by the graphs in Figures 3.8 and 3.9, the kick applied to the trajectory of initial point $x_0 = 75.515...$ changes after running for $t = 7$, after this time the kick that is applied is κ_T with $\kappa_T = \frac{1}{4}\kappa$. The flow-kick process starts afresh from time T on, only from a different initial value which is still above the Allee threshold, namely $\tilde{x}_0 = G_T(x_0)$, and for a different (fixed) disturbance (τ, κ_T). Since we observe that the x-position of the blue trajectory converges to a convergence interval after $T = 7$, this new initial value is contained in I_1 when this interval would have been constructed for (τ, κ_T).

However, when κ_T would have been changed differently, the system might still not have been able to recover in time τ from $-\kappa_T$, if this disturbance had been initiated at $\tilde{x}_0$. This happens when a kick is altered either too late, too little or both. This is the instance for the red flow-kick trajectory in Figure 3.9. After $T = 7$ the original kick, $\kappa = -16$, is divided by two, which gives $\kappa_T = -8$ for unaltered flow time $\tau = 1$. Although the kick now is considerably smaller than before, the flow time, $\tau = 1$, stays smaller than the minimal time it takes for the system to recover from $-\kappa_T$. In other words, for all $x \in (A + |\kappa_T|, \tilde{x}_0)$ we ensure with the fact that $f \in C^1$ that

$$1 = \tau < \int_{x-|\kappa_T|}^{x} \frac{1}{f(x)} dx = \int_{x-|\kappa_T|}^{x} \frac{1}{rx\left(\frac{x}{A} - 1\right)\left(1 - \frac{x}{C}\right)} dx,$$

by calculating this integral for $x = \tilde{x}_0$ and x approaches $A + |\kappa_T|$. In this case, the latter integral diverges as, since we divide by $\frac{x}{A} - 1$. However, it is not always the case that the divergence of the integrand guarantees convergence of the integral. For $r = \frac{1}{2}$, $A = 50$ and $C = 200$, we find, with *flowkick.py*, the value of $\tilde{x}_0 = 64.052...$ and that

$$\int_{\tilde{x}_0-|\kappa|}^{\tilde{x}_0} \frac{1}{rx\left(\frac{x}{A} - 1\right)\left(1 - \frac{x}{C}\right)} dx = \int_{56.052...}^{64.052...} \frac{1}{rx\left(\frac{x}{A} - 1\right)\left(1 - \frac{x}{C}\right)} dx = 2.017... > 1.$$

The flow-kick trajectory of $(\tau, K(t))$ with

$$K(t) = \begin{cases} -16 & \text{for } 0 \leq t < 7 \\ -8 & \text{for } t \geq 7 \end{cases},$$

is thus unstable. Changing this definition of K to

$$K(t) = \begin{cases} -16 & \text{for } 0 \leq t < 4 \\ -8 & \text{for } t \geq 4 \end{cases},$$

leads contrarily to a stable flow-kick trajectory for disturbance $(\tau, K(t))$ with a different initial value $\tilde{\tilde{x}}_0 = 80.359....$ This initial value yields

$$\int_{\tilde{\tilde{x}}_0-|\kappa|}^{\tilde{\tilde{x}}_0} \frac{1}{rx\left(\frac{x}{A} - 1\right)\left(1 - \frac{x}{C}\right)} dx = \int_{72.359...}^{80.359...} \frac{1}{rx\left(\frac{x}{A} - 1\right)\left(1 - \frac{x}{C}\right)} dx = 0.649... < 1.$$

The system can consequently recover from the changed disturbance $(\tau, K(t))$ in the indicated flow-time if the kick size is adjusted early enough.

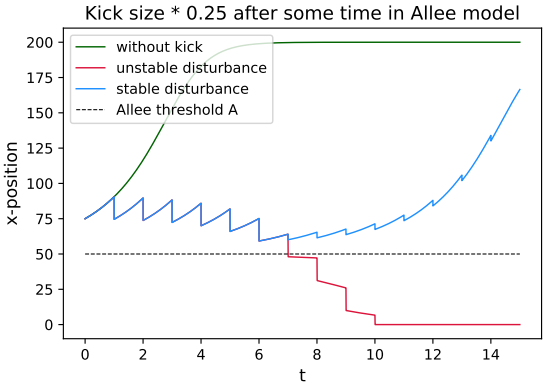

***Figure 3.8:** After $T = 7$ the kick size of the blue trajectory is four times smaller than before which leads to a stable situation. The kick applied to the red trajectory does not depend on time.*

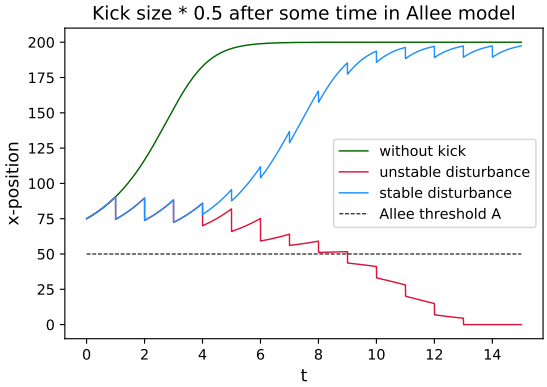

***Figure 3.9:** After $T = 4$ the kick applied to the blue flow-kick trajectory is bisected. In contrast to the red trajectory where this is done at a later moment, at $T = 7$, the blue trajectory remains in $\mathcal{B}(x_*)$.*

4 Two-dimensional flow-kick systems

In one-dimensional flow-kick systems the choice of kick is restricted by the fact that the phase space is a line. The only thing that can be determined is therefore the size of the kick, which can be positive or negative. In n-dimensional systems the possibility to apply kicks in other directions broadens our horizon and makes it possible to extend some previous definitions. To embroider on the definitions from Chapter 2 we consider the undisturbed dynamics of the two-dimensional system defined by

$$f(x) = \begin{cases} \dot{x} &= -x - y + \cos(x) \\ \dot{y} &= \sin(x) \end{cases}, \tag{4.1}$$

see Figure 4.1. This figure is plotted by means of the application `pplane` written for Java. The complexity of the phase plane of this systems raises several questions regarding the stability of disturbances. For equilibria of (4.1) holds that $\dot{x} = 0$ and $\dot{y} = \sin(x) = 0$. From the latter equality follows that x-coordinates of equilibria are given by $x = k\pi$ with $k \in \mathbb{Z}$. Combining this with the former equality yields

$$\begin{aligned} 0 &= \dot{x} \\ &= -x - y + \cos(x) \\ &= -k\pi - y + \cos(k\pi) \\ &= -k\pi - y + (-1)^k. \end{aligned}$$

Consequently, equilibria are given by $(x, y) = (k\pi, -k\pi + (-1)^k)$ with $k \in \mathbb{Z}$. Consider the basin of attraction of $\tilde{x}_* = (-2\pi, 2\pi + 1)$, $\mathcal{B}(\tilde{x}_*)$, highlighted in orange in Figure 4.1. If the length of a kick in a disturbance applied from initial value x_*, $|\kappa| = \sqrt{\kappa_1^2 + \ldots + \kappa_n^2}$, is fixed and the direction of κ varies, the effect of the kick direction can be studied. This is covered in the following sections, as well as the higher dimension of the phase space of the flow-kick dynamics that makes it less apparent what it means to recover from a disturbance in comparison to recovering in one-dimensional flow-kick systems. Another question arising for two-dimensional systems is whether there always is a kick for a certain recovery time for which the flow-kick trajectory stays in a neighborhood of an asymptotically stable equilibrium. This question is studied in Section 4.3.

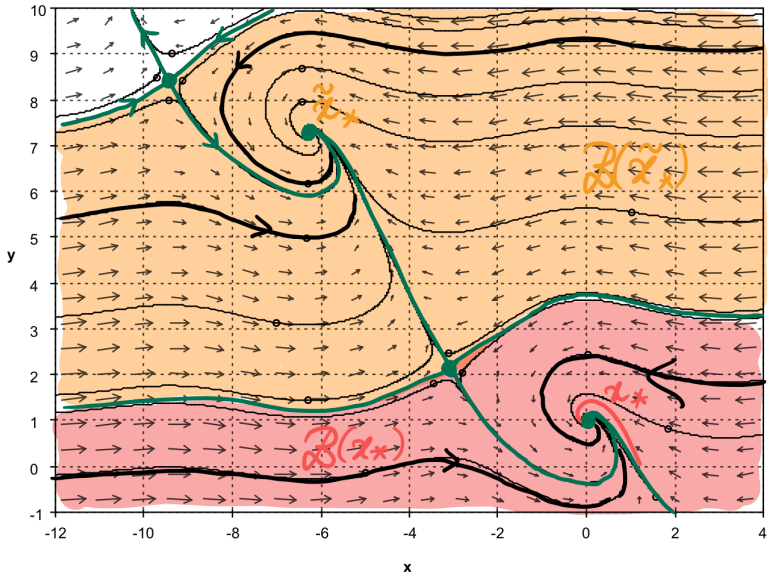

Figure 4.1: Phase plane of (4.1) ***with basins of attraction of asymptotically stable equilibria*** x_* ***and*** $\tilde{x}_*$ ***indicated by red respectively orange.***

4.1 Resilient and non-resilient sets

Resilient and non-resilient regions in n-dimensional flow-kick systems with $n \geq 2$, see Definition 3.2, are analogous to their one-dimensional equivalents.

Definition 4.1. *The resilient set for a point $x_0 \in \mathcal{B}(a)$, $R^s_{x_0}$, contains all disturbance pairs (τ, κ) with $\tau \in \mathbb{R}_{>0}$ and $\kappa \in \mathbb{R}^n$ for which the flow-kick trajectory initiated at x_0 remains in $\mathcal{B}(a) \subseteq \mathbb{R}^n$. This resilient set is separated from the non-resilient set for a point $x_0 \in \mathcal{B}(a)$, $R^u_{x_0}$, which contains all the disturbances for which there exists a $T > 0$ such that the flow-kick trajectory of disturbance (τ, κ) escapes from $\mathcal{B}(a)$, by the resilience boundary of x_0, R_{x_0}.*

Definition 4.2. *A n-dimensional system is said to be able to recover from a disturbance (τ, κ) initiated at $x_0 \in \mathcal{B}(a)$ with $\kappa \in \mathbb{R}^n$, if there is an $i \in \mathbb{Z}_{\geq 1}$ such that there exists an orbit between $\phi_\tau(G^{i-1}_{\tau,\kappa}(x_0))$ and $G^i_{\tau,\kappa}(x_0)$ in the phase space defined by (2.2) such that flowing forward for time τ after applying kick κ results in the same position in the phase plane as before applying κ to the system. In other words, for some $i \in \mathbb{Z}_{\geq 1}$ holds that*

$$\phi_\tau(G^i_{\tau,\kappa}(x_0)) = G^{i-1}_{\tau,\kappa}(x_0).$$

This means that the system can only recover from kick κ when there is at least a $t_0 \geq 0$ such $(t_0, t_0 + \tau) \subseteq \mathbb{R}_{\geq 0}$ and a $X_0 \in \mathcal{B}(a)$ such that for the end points of a segment of the forward orbit of X_0,

$$\{\phi_t(X_0) : t \in (t_0, t_0 + \tau)\} \subseteq \Gamma^+(X_0) = \{\phi_t(X_0) : t \geq 0\},$$

we have that

$$\phi_{t_0}(X_0) - \phi_{t_0+\tau}(X_0) = \kappa.$$

Even though this thesis mainly focuses on disturbances applied to systems with asymptotically stable equilibria in their undisturbed dynamics, these orbit segments can also be constructed for unstable nodes, unstable focuses or stable equilibria in undisturbed systems. For equilibria that are stable but not asymptotically stable we only pursue the hyperbolic situation, thus, a stable center equilibrium. Further analysis of these non-hyperbolic equilibria is unfortunately not in the range of this thesis, but will be discussed in short in Chapter 8.

4.2 Linear undisturbed dynamics

A hyperbolic equilibrium x_* in a nonlinear system is topologically conjugate to its linearization on a neighborhood N of x_*, by Theorem 2.1. Understanding how disturbances in linear systems behave, is therefore useful. Periodic orbits can be obtained by applying very specific kicks, which is explained in the following paragraphs.

For all unstable nodes the real eigenvalues are greater than zero. We obtain three situations for $n = 2$. To start, assume that the eigenvalues λ_1 and λ_2 are equal with two linearly independent eigenvectors v_1 and v_2, see Figure 4.2. The orbit of every solution in this linear system is a half-line and can be written in the form $x(t) = e^{\lambda t}(c_1 v_1 + c_2 v_2)$ for constants c_1 and c_2 and for all choices of c_1 and c_2 the set of vectors $\{c_1 v_1 + c_2, v_2\}$ cover every direction in the (x, y)-plane. Hence, for every $\kappa \in \mathbb{R}^2$ there exists a X_0 for which there is an orbit segment $\{\phi_t(X_0) : t \in (t_0, t_0 + \tau)\}$, part of a half-line with direction $c_1 v_1 + c_2 v_2 = -\kappa$, such that $\phi_{t_0}(X_0) - \phi_{t_0+\tau}(X_0) = \kappa$. In Figure 4.2 these orbit segments are highlighted in blue for two initial values X_0 and $\tilde{X}_0$.

Consider the unstable saddle point with eigenvalues $\lambda_1 < 0 < \lambda_2$ and two distinct eigenvectors, see Figure 4.3. Solutions of the system are given by $x(t) = c_1 e^{\lambda_1 t} v_1 + c_2 e^{\lambda_2 t} v_2$. Let X_0 be the desired value at which the flow-kick trajectory is initiated and the initial value of the problem, so $X_0 = x(0)$. The kick for which there exists a time-interval $(t_0, t_0 + \tau) = (0, \tau)$ for this

X_0, is given by $\kappa = \phi_0(X_0) - \phi_\tau(X_0) = X_0 - \phi_\tau(X_0)$. The system can therefore recover from disturbance $(\tau, X_0 - \phi_\tau(X_0))$ if the flow-kick trajectory is initiated at $\phi_\tau(X_0)$. Via the same way we can find a κ for a X_0 if the equilibrium is an unstable node as depicted in Figures 4.4 and 4.5 (or a stable center, see Figure 4.6). For eigenvalues with nonzero imaginary part (focus points), disturbances from which the system can recover can be constructed the same way as for unstable saddle points.

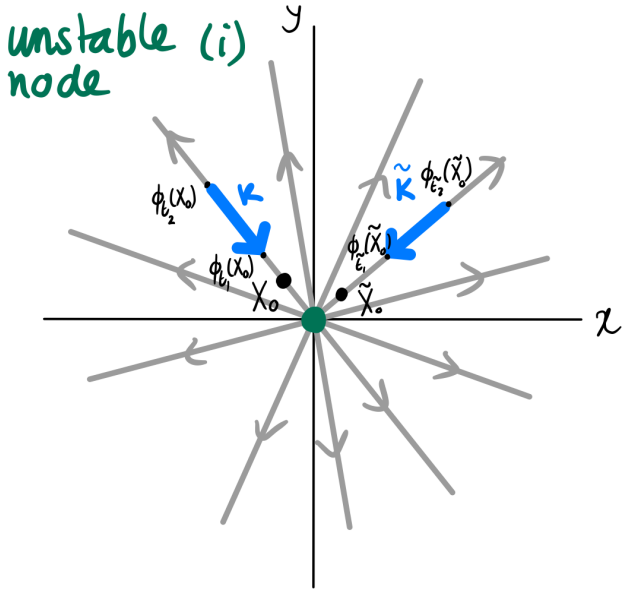

Figure 4.2: For an unstable node with one eigenvalue with multiplicity two, there is a X_0 and an interval $(t_1, t_2) \subseteq \mathbb{R}_{>0}$ with length $\tau \in \mathbb{R}$ for which $\phi_{t_1}(X_0) - \phi_{t_2}(X_0) = \kappa$ for all $\kappa \in \mathbb{R}^2$.

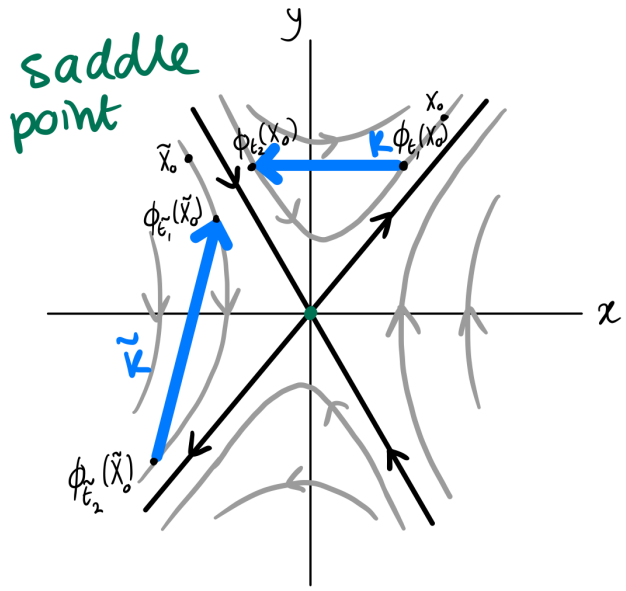

Figure 4.3: A kick κ can be determined for an unstable saddle point equilibrium with real eigenvalues $\lambda_1 < 0 < \lambda_2$ for all initial values $X_0 \in \mathbb{R}^2$ and flow times τ.

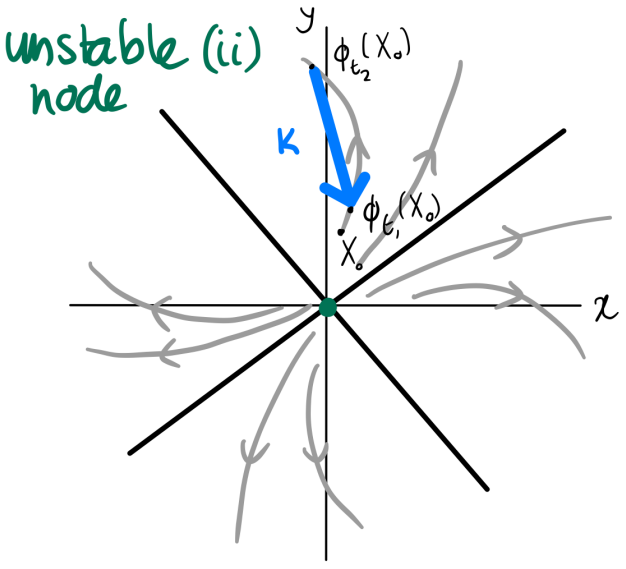

Figure 4.4: A kick κ can be determined for an unstable node with two distinct eigenvalues with a method analogous to the one for saddle points .

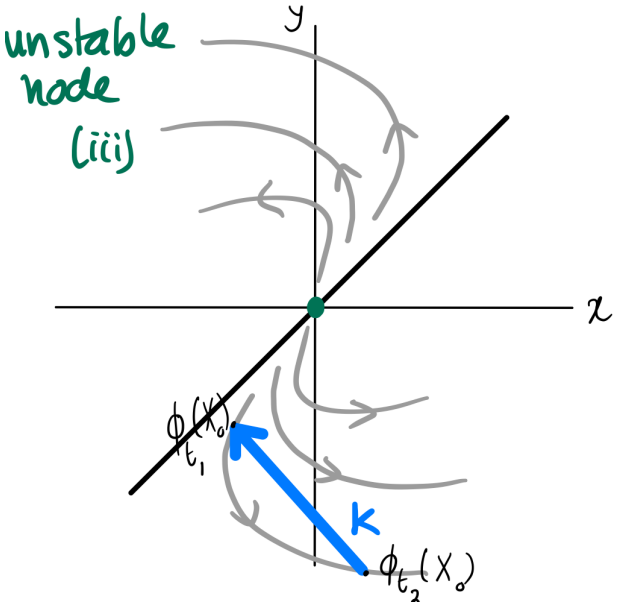

Figure 4.5: For an unstable node with two eigenvalues but only two eigenvectors a kick κ can be found the same way as for the unstable node in Figure 4.4.

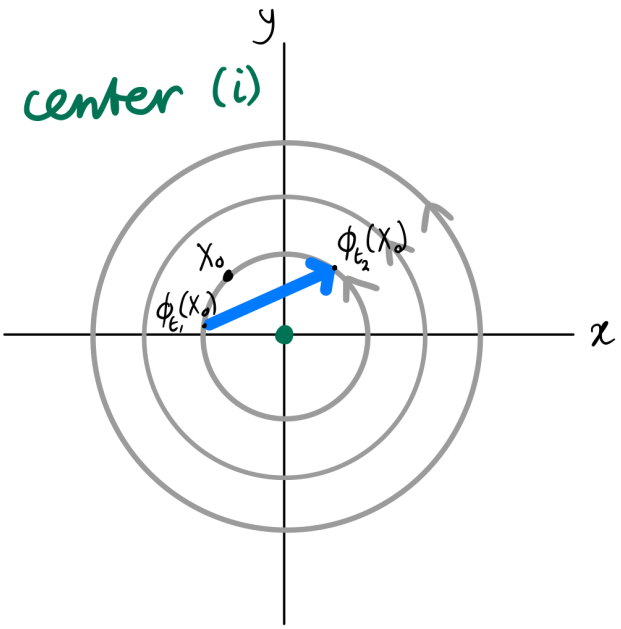

***Figure 4.6:** For all κ around a stable center there exists a X_0 such that we obtain a periodic flow-kick trajectory.*

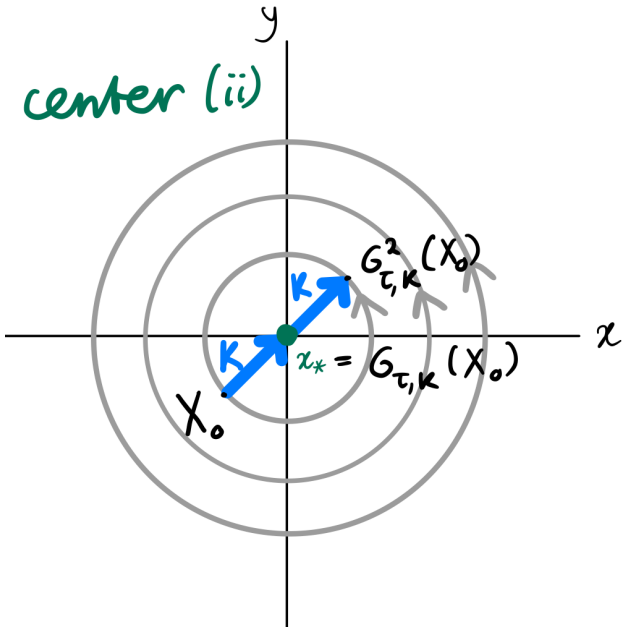

***Figure 4.7:** A periodic flow-kick trajectory via center equilibrium x_* such that flow-kick trajectory stays in equilibrium for τ.*

Stable but not asymptotically stable equilibria are often found in systems with non-hyperbolic equilibria and open up a whole new world of flow-kick dynamics then examined so far. A sneak preview is given in Figures 4.6 and 4.7. In Figure 4.6 the situation is comparable with the one from the unstable saddles and nodes. For any disturbance (κ, τ) there exists a initial value for the flow-kick trajectory such that there is an orbit between the end points of $\{\phi_t(X_0) : t \in (t_0, t_0+\tau)\}$ with $\phi_{t_0}(X_0) - \phi_{t_0+\tau}(X_0) = \kappa$. Figure 4.7 is on the other hand more exotic. Note that kick κ is applied twice from initial value X_0 on and that the flow-kick trajectory passes through stable equilibrium $x_* = G_{\tau,\kappa}(X_0)$. The obtained periodic flow-kick orbit consists of four actions: applying κ from X_0 on to x_*; staying for time τ at x_*, since $\dot{x} = 0$ for x_*; applying κ another time, from x_* to $G^2_{\tau,\kappa}(X_0)$; and flowing back from $G^2_{\tau,\kappa}(X_0)$ to X_0. In this manner the stable disturbance (τ, κ) is not instant anymore and takes time τ, as if someone "pressed pause" for τ in the middle of the execution of the kick. Chapter 8 elaborates a bit on this observation.

4.3 Nonlinear undisturbed dynamics

The disturbances in the previous section were applied to linear dynamical systems. Theorem 2.1 states that for a hyperbolic equilibrium x_* of (2.1) there exists a neighborhood N of x_* such that the dynamics in the nonlinear is topologically conjugate to its linearization in this neighborhood. Some interesting observations about flow-kick dynamics in nonlinear systems can now be derived in N.

Theorem 4.1. *For an asymptotically stable equilibrium x_* of a system given by $\dot{x} = f(x)$ and a certain recovery time τ there exists a kick $\kappa \neq 0$ such that the flow-kick trajectory of x_* stays in a neighborhood N of x_* for $t \geq T$ with $T \geq 0$.*

Proof. With Theorem 2.1 there exists a neighborhood M of asymptotically stable equilibrium x_* such that the flow is topologically conjugate for homeomorphism $h : \mathbb{R}^n \to \mathbb{R}^n$ to its linearization on M. Note that all eigenvalues of $Df(x_*)$ are, by assumption, strictly smaller than zero. Consequently, we have that $x_* = \lim_{t\to\infty} \phi_t(x)$ for all $x \in h(M)$. This yields a compact subset of $h(M)$ denoted by V such that for all $t > 0$ and all $x \in V$ holds that $\phi_t(x) \in V$, which gives

that V is a trapping region. Assume that $x_0 \in \partial V$. Let x_0 be the initial value of the problem $\dot{x} = Df(x)$ and let $y_0 : \mathbb{R} \to \mathbb{R}^n$ be the associated solution for this x_0. Consider

$$I := \min_{x_0 \in \partial V} \int_0^\tau y_0(t)dt, \tag{4.2}$$

and a neighborhood

$$\tilde{N} := \{x \in V : d(x, \partial V) > I\}$$

of x_*. For all $x \in \tilde{N}$ the flow-kick trajectory, defined by disturbance (τ, κ) such that $|\kappa| < I$, will definitely return to $\tilde{N}$, because the distance between $\phi_t(x)$ and x_* decreases by the solutions of the linearization. However, if $x \in V \setminus \tilde{N}$ we cannot guarantee this return. The flow-kick trajectory can, namely, be "kicked out" of trapping region V. Since h is a homeomorphism we can translate these sets with their properties to the nonlinearized system. This gives that there exists a kick $\kappa \neq 0$ such that the flow-kick trajectory of x_* stays in neighborhood $N := h^{-1}(\tilde{N})$ of x_* for all $t \geq 0$. □

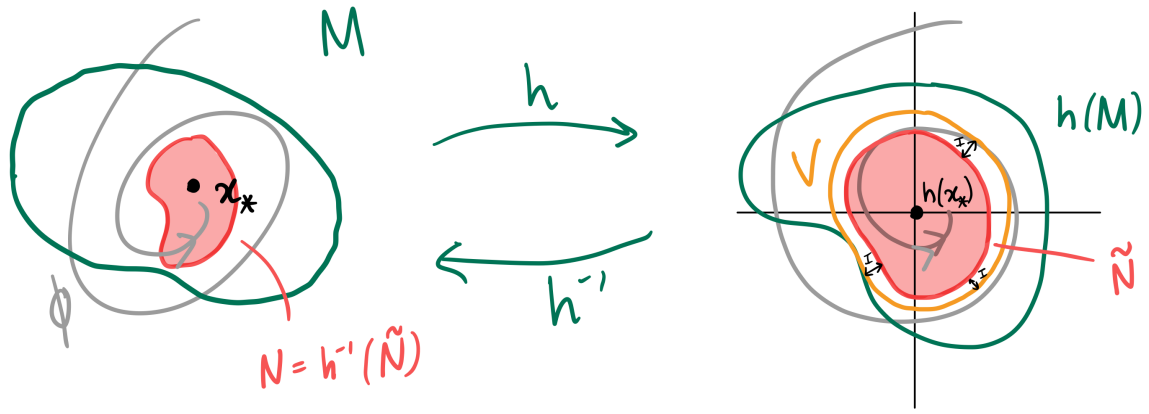

Figure 4.8: Sketch of proof of Theorem 4.1. On the left the nonlinear system is depicted and on the right the linearized version.

Figure 4.8 illustrates the proof and Figure 4.9 depicts the construction of $\tilde{N}$, about which the following remarks need to be made. Note that N, in the nonlinear system, might not be the biggest neighborhood for which there exists an $\kappa \neq 0$ such that the flow-kick trajectory of an asymptotically stable equilibrium stays in N. Consider $X = \{\phi_\tau(x) : x \in \partial V\}$, black in Figure 4.9. To illustrate this, $\tilde{x}_0 \in \partial V$ is indicated in Figure 4.9 in blue. The distance between $\tilde{x}_0 \in \partial V$ and $\phi_\tau(\tilde{x}_0) \in X$ is larger than the distance between $x_0 \in \partial V$ and $\phi_\tau(x_0) \in X$, in other words, $d(\tilde{x}_0, \phi_\tau(\tilde{x}_0)) > d(x_0, \phi_\tau(x_0))$. There follows that $I \leq d(x_0, \phi_\tau(x_0))$. Assume that (4.2) is minimal for $x_0 \in \partial V$ and $\phi_\tau(x_0)$ highlighted in green in Figure 4.9. For this x_0, which does not have to be unique, $\phi_t(x_0) - x_0$ does not have to be perpendicular to the tangent space of V in x_0. If this were the case, $\tilde{N}$ would be maximal. If this angle, α, would not be right, it could be taken into consideration by defining $\tilde{N} = \{x \in V : d(x, \partial V) > I \sin(\alpha)\}$. After applying h^{-1} to $\tilde{N}$, we now obtain a larger neighborhood N of x_* for which there exists a κ with $|\kappa| < I$ such that the flow-kick trajectory will stay in N after time $t \geq T$.

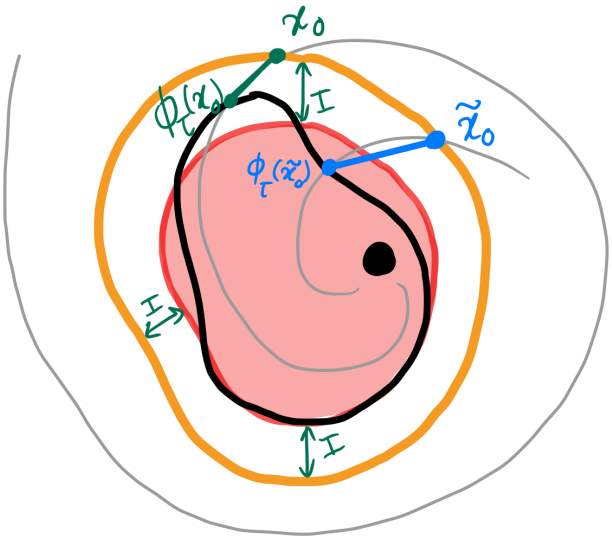

Figure 4.9: Construction of $\tilde{N}$, in red, in proof of Theorem 4.1. V is orange.

4.4 Numerical results

Figures 10(a) and 10(b) are plotted by *flowpush.py* from Appendix A.2. As in the one-dimensional version, kick κ is applied based on the index of `t` and flow time τ. In two dimensions this is done by appending `xG1[-1] + dt*f1(xG1[-1],xG2[-1])` to the array `xG1` that stores the values of the first coordinate and appending `xG2[-1] + dt*f1(xG1[-1],xG2[-1])` to `xG2` for defining what happens to the second coordinate. In this case, `f1` and `f2` are the coordinate functions of a two-dimensional system, for the one-dimensional case `f2` does not exist and `f1` only has one argument. The three-dimensional case is approached in a similar way. The numerical results from this section illustrate the influence of kick direction.

In Table 4.1 the input values are stated for the flow-kick trajectories and undisturbed orbit depicted in the Figures 10(a) and 10(b), which compare a vertical and horizontal disturbance to the same initial value of (4.1). For the horizontal disturbance, the flow-kick trajectory of $(x_0, y_0) = (0.386..., 0.773...)$ stays inside the basin of attraction of the asymptotically stable equilibrium x_* from (4.1). On the other hand, the flow-kick trajectory for the vertical disturbance escapes from $\mathcal{B}(x_*)$

Initial value (x_0, y_0)	Flow time τ	Kick κ	Stability of orbit	See Figure 4.10
$(0.386..., 0.773...)$	–	0	Stable	In red
$(0.386..., 0.773...)$	0.5	$(0.5, 0)$	Stable	(a)
$(0.386..., 0.773...)$	0.5	(0.469...,0.171...)	Stable	(c)
$(0.386..., 0.773...)$	0.5	(0.383...,0.321...)	Stable	(d)
$(0.386..., 0.773...)$	0.5	(0.25,0.433...)	Unstable	(e)
$(0.386..., 0.773...)$	0.5	$(0, 0.5)$	Unstable	(b)

***Table 4.1: Some results for numerical analysis of* (4.1).**

In Figure 10(a) a horizontal stable disturbance given by $(0.5; (0.5, 0))$ is applied to initial value $x_0 = (0.386..., 0.773...)$ for the system defined by (4.1). For this disturbance, the flow-kick trajectory stays in $\mathcal{B}(x_*)$.

Figure 10(b) portrays a vertical unstable disturbance applied to the same system. The red orbits in both figures are the same, but since the disturbance $(0.5; (0, 0.5))$ makes the flow-kick trajectory of x_0 escape the basin of attraction of x_*, see 4.1, it appears as if the orbits have different size. Figure 4.1 also depicts orbit in red in $\mathcal{B}(x_*)$. For Figure 10(c) until 10(e) the kick

magnitude of κ, $|\kappa|$, is fixed on 0.5. The direction is adjusted by rotating over 20 degrees. For an angle γ somewhere between 40 and 60 degrees the flow-kick trajectory escapes from the basin of attraction. By applying all possible disturbances to the initial value $x_0 = (0.386..., 0.773...)$ we would be able to construct a resilience boundary for x_0. See Chapter 8 for more information on the construction of this resilience boundary.

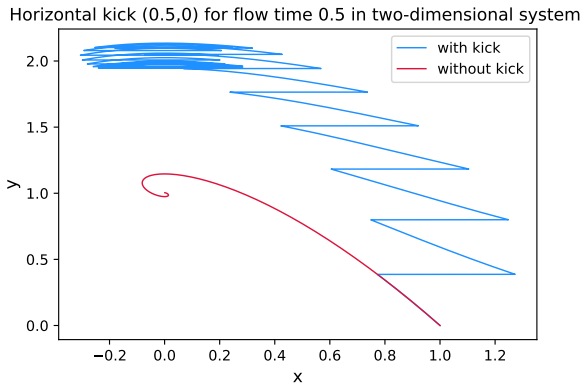

(a) Horizontal disturbance

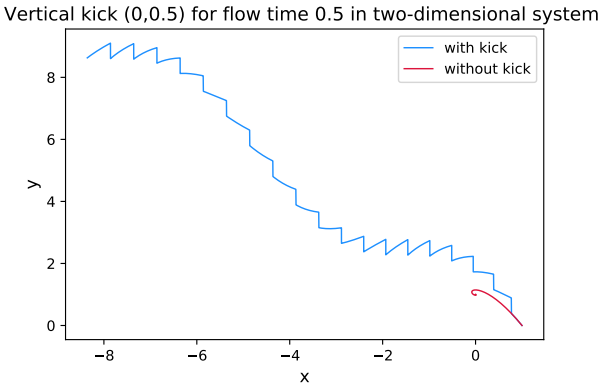

(b) Vertical disturbance

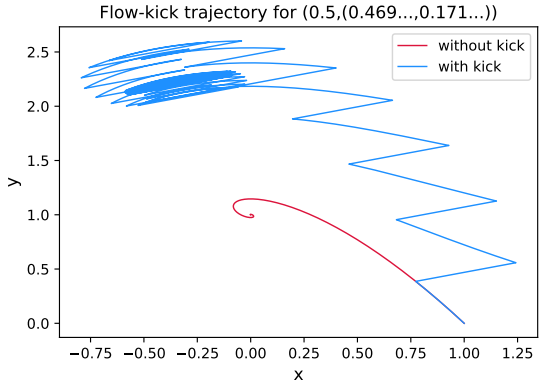

(c) Angle of kick is 20°

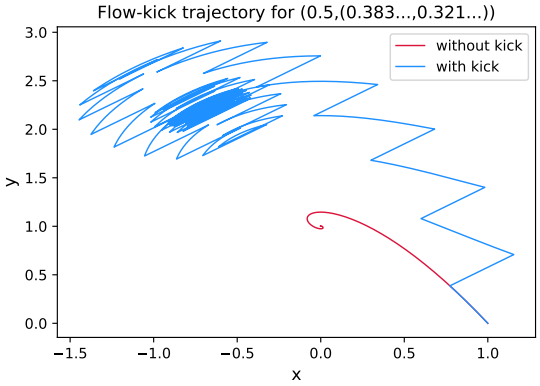

(d) Angle of kick is 40°

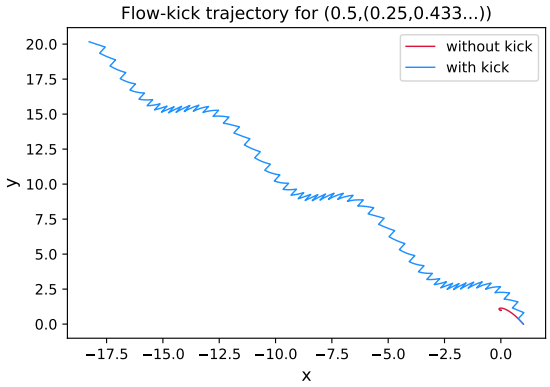

(e) Angle of kick is 60°

Figure 4.10: Disturbances with $|\kappa| = \frac{1}{2}$ ***applied to undisturbed dynamics of*** (4.1) ***for initial value*** $x_0 = (0.386..., 0.773...)$.

5 Flow-push dynamics

In the previous chapters, it was assumed that a kick is an instant change to a dynamical system. However, sometimes it is not realistic to assume this, a wildfire, for instance, can for example take longer than a week and then this time might not be negligible in proportion to the time it takes for the system to recover. Therefore, this section covers "pushes", disturbances that are not instant and have a certain duration, and their induced flow-push dynamics.

5.1 Definition

Flow-push systems can be defined in more than one way. This depends on how the push is approached. The push can be explicitly added to the undisturbed dynamics, see Definition 5.1, or be considered as an internal property of a system such that it is more implicitly (de)activated when time continues, see Definition 5.2.

Definition 5.1. *A flow-push system, $P : \mathbb{R}^n \times \mathbb{R} \to \mathbb{R}^n$, for $x \in \mathbb{R}^n$, $t \in \mathbb{R}$, triplet (τ, τ_p, κ) and sufficiently smooth push $p : [0, \tau_p) \to \mathbb{R}^n$ given by $t \mapsto \begin{pmatrix} p_1(t) \\ \vdots \\ p_n(t) \end{pmatrix}$ such that*

$$\int_0^{\tau_p} p_i(t)dt = \kappa_i,$$

with κ_i the i-th coordinate of an instant kick κ, p_i the i-th coordinate function of p, τ_p the time over which the push is applied to a system of ordinary differential equations given by $\dot{x} = f(x)$, and recovery time $\tau - \tau_p \geq 0$, is defined by

$$P_{\tau,\tau_p,\kappa}(x,t) = \begin{cases} \dot{x}_1 &= f_1(x) + p_1(t \mod \tau) \\ \dot{x}_2 &= f_2(x) + p_2(t \mod \tau) \\ \vdots & \quad \vdots \\ \dot{x}_n &= f_n(x) + p_n(t \mod \tau) \end{cases}, \text{ for } t \mod \tau \in [0, \tau_p).$$

For $t \mod \tau \in [\tau_p, \tau)$ the flow-push system is defined by the original system given by $\dot{x} = f(x)$.

In this case, the push is only defined on the interval when it is actually applied, so for $t \mod \tau \in [0, \tau_p)$. This is instead of switching the push on when $t \in [j\tau, j\tau + t_p)$ and off when $t \in [j\tau + \tau_p, (j+1)\tau)$ for $j \in \mathbb{Z}_{\geq 0}$ for $t \geq 0$.

Definition 5.2. *A flow-push system, $\tilde{P} : \mathbb{R}^n \times \mathbb{R} \to \mathbb{R}^n$, is defined for $x \in \mathbb{R}^n$, $t \in \mathbb{R}$, and triplet (τ, τ_p, κ) of kick $\kappa \in \mathbb{R}^n$, push time τ_p and recovery time $\tau - \tau_p \geq 0$ by*

$$\tilde{P}_{\tau,\tau_p,\kappa}(x,t) = \begin{cases} \dot{x}_1 &= f_1(x) + \tilde{p}_1(t) \\ \dot{x}_2 &= f_2(x) + \tilde{p}_2(t) \\ \vdots & \quad \vdots \\ \dot{x}_n &= f_n(x) + \tilde{p}_n(t) \end{cases},$$

with $\tilde{p} : \mathbb{R}_{\geq 0} \to \mathbb{R}^n$ given by $t \mapsto \begin{pmatrix} \tilde{p}_1(t) \\ \vdots \\ \tilde{p}_n(t) \end{pmatrix}$ such that $\tilde{p}$ is sufficiently smooth on $[j\tau, j\tau + j\tau_p)$ for all $j \in \mathbb{Z}_{\geq 0}$ and that for all $i \in \{1, \ldots, n\}$ holds that $\tilde{p}_i(t) = 0$ for $t \mod \tau \in [\tau_p, \tau)$. Besides, for all $j \in \mathbb{Z}_{\geq 0}$ holds that

$$\int_{j\tau}^{j\tau+\tau_p} \tilde{p}_i(t)dt = \kappa_i.$$

If $p_i(0) = p_i(\tau_p) = 0$ and $\tilde{p}_i(j\tau) = \tilde{p}_i(\tau_p + j\tau) = 0$ for all $i \in \{1, \ldots, n\}$ and $j \in \mathbb{Z}_{\geq 0}$, flow-push systems are continuously differentiable. In this thesis, we have not yet considered the non-homogeneous pushes. Applying a homogeneous push p continuously gives that

$$p_i(t) = \frac{p_i}{\tau_p},$$

since

$$\int_0^{\tau_p} \frac{p_i}{\tau_p}\, dt = \left[\frac{p_i}{\tau_p} t\right]_0^{\tau_p} = p_i.$$

Note that a kick κ would be a push p with $\tau_p = 0$, this gives

$$\lim_{\tau_p \to 0} \int_0^{\tau_p} \frac{p_i}{\tau_p}\, dt = \lim_{\tau_p \to 0} \left[\frac{p_i}{\tau_p} t\right]_0^{\tau_p} = \lim_{\tau_p \to 0} p_i - 0 = p_i.$$

This gives that $\int_0^{\tau_p} p_i(t)dt = \kappa_i$. We should also remark that $\tau - \tau_p \geq 0$, since the system should be able to recover from a disturbance before a new disturbance kicks in. If $\tau - \tau_p < 0$ the intensity of the push would increased after τ which, in some real-life examples, is not even possible. Consider for example wildfires. If $\tau - \tau_p < 0$ the original fire would not have been extinguished before the second fire starts. In other real-life examples it might however be possible to apply new pushes before the old ones are worn off. The concentration rate of pollution with chemicals in a lake can for example increase, when two different contaminating loads are leaking into it at the same time.

5.2 Numerical results

The situation for $\tau - \tau_p < 0$ can be approached in two different ways. In the first case, the impact of the pushes piles up after flow time τ passed and an extra push is applied. In the second case, a new push is applied at τ and the previous push is overwritten by this new push. The Python code *flowpush-trajplot.py* in Appendix A.2 does not explicitly exclude pushes for which $\tau - \tau_p < 0$. Both the old and new push are defined by (τ, τ_p, κ). When analyzing system numerically, homogeneous pushes come down to adding

$$p/\frac{\tau_p}{dt},$$

for τ_p/dt time steps of size dt, this way we have $\sum_{n=1}^{\frac{\tau_p}{dt}} p/\frac{\tau_p}{dt} = \frac{\tau_p}{dt} \cdot p/\frac{\tau_p}{dt} = p$, and as before a kick κ would be a push p with $\tau_p = 0$. Thus, $\sum_{n=1}^{\frac{\tau_p}{dt}} p/\frac{\tau_p}{dt} = \kappa$. When $\tau - \tau_p < 0$ the old push is overwritten by the new one in the code. Note that $\frac{p_i}{\tau_p} < \frac{p_i}{\tau}$, so the applied push is in total strictly smaller than κ. We have

$$\sum_{n=1}^{\frac{\tau}{dt}} \frac{p}{\frac{\tau_p}{dt}} = \frac{\tau}{dt}\frac{p}{\frac{\tau_p}{dt}} = \frac{\tau}{\tau_p} p < p = \kappa,$$

and not equal to κ. Pushes for which $\tau - \tau_p < 0$ given by (τ, τ_p, κ) can now be rewritten to pushes defined by $(\tau, \tilde{\tau}_p, \tilde{\kappa})$ with $\tilde{\tau}_p = \tau$ and $\tilde{\kappa} = \frac{\tau}{\tau_p}\kappa$, so that these pushes meet the requirement that

$$\int_0^{\tau_p} p_i(t)dt = \kappa_i,$$

from Definitions 5.1 and 5.2, see Figures 5.1 and 5.2.

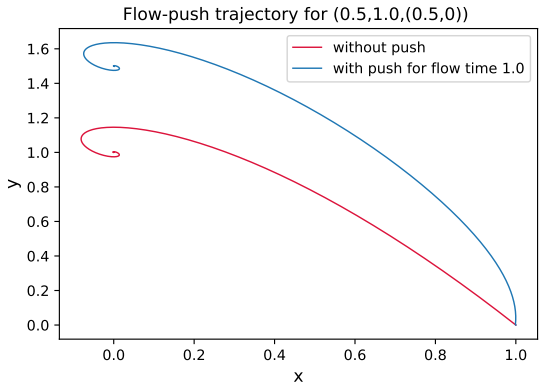

Figure 5.1: Push with $\tau - \tau_p < 0$ ***in system given by*** $\{\dot{x} = -x - y + \cos(x), \dot{y} = \sin(x)\}$.

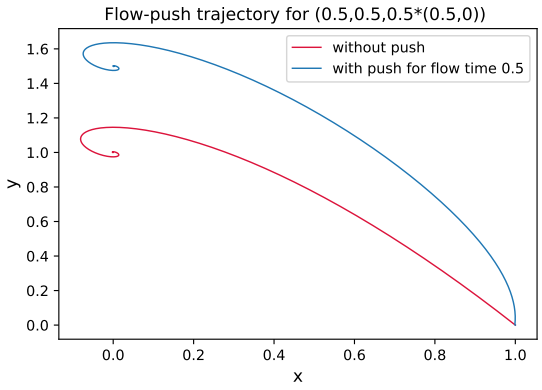

Figure 5.2: Redefining push from 5.1 such that $\tau - \tau_p = 0$ ***and that Definition 5.1 holds, the push is defined by*** $\left(\frac{1}{2}, \frac{1}{2}, \frac{1}{2}\left(\frac{1}{2}, 0\right)\right)$.

In Figure 5.4 the effect of an increasing push time in a linear system is depicted. The undisturbed dynamics of the linear system are given by

$$\begin{cases} \dot{x} = -x - y \\ \dot{y} = -x \end{cases}. \tag{5.1}$$

The pushes are all defined by the same flow time τ and same kick κ, the flow-push trajectories are all initiated at the same value $(x_0, y_0) = (0.0502..., -0.0016...)$. See Figure 5.3 for the flow-kick trajectory defined by (τ, κ). Note that the size of the red orbit in the undisturbed dynamics stays the same size in all six figures, this way we can compare the orbits.

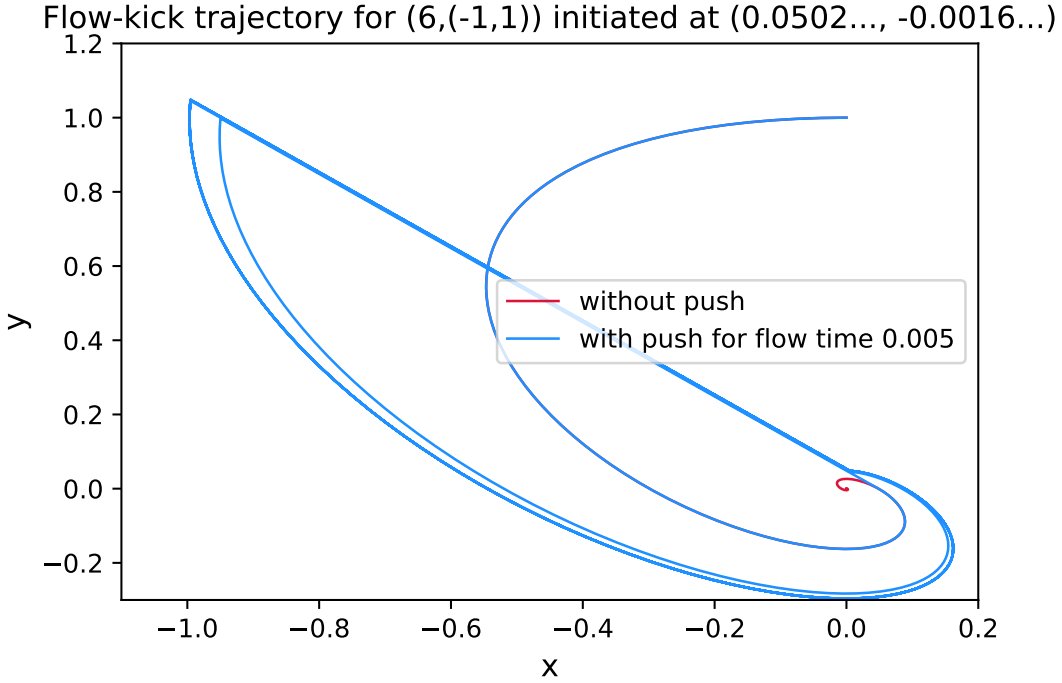

Figure 5.3: Disturbance $(\tau, \kappa) = (6, (-1, 1))$ ***initiated at*** $(0.0502..., -0.0016)...$ ***is shown here for the system given by*** (5.1).

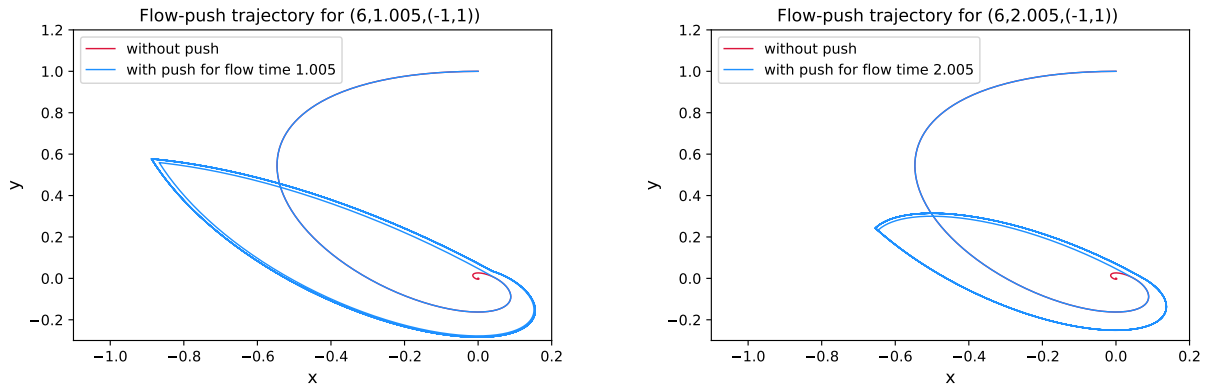

(a)

(b)

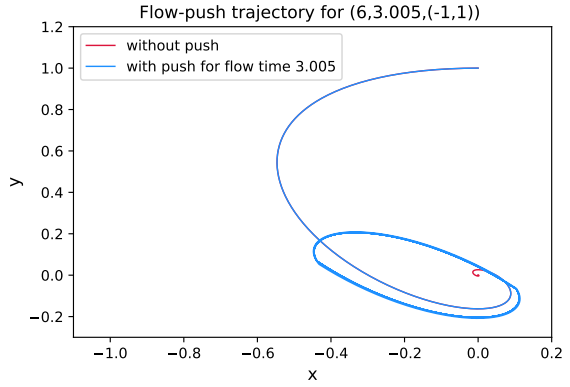

(c)

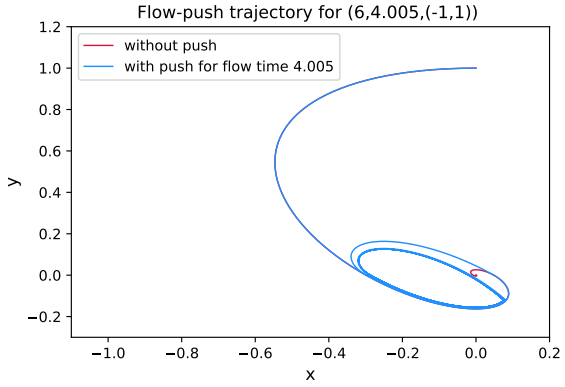

(d)

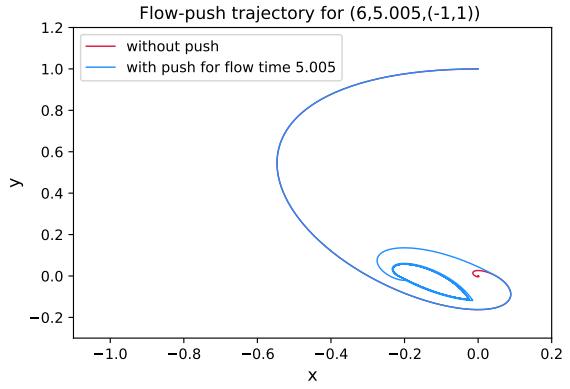

(e)

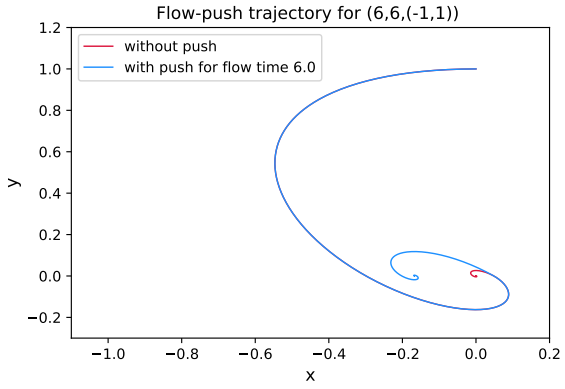

(f)

Figure 5.4: Flow-push trajectories initiated at $(0.0502..., -0.0016...)$ ***for the push defined by*** $(\tau, \tau_p, \kappa) = (6, \tau_p, (-1, 1))$ ***with*** τ_p ***increasing from 0.005 until 6 on the undisturbed dynamics given by*** (5.1)**.**

The more the push time increases towards the flow time, the smaller the flow-push orbits get in comparison to the orbit of the initial value in the undisturbed dynamics. Besides this, the obtained trajectories all appear to become periodic when time continues. This observation is not extremely surprising, when taking Definition 4.2 in consideration. As flow-push systems are an extension of flow-kick systems, the notion of recovering can also be translated from flow-kick to flow-push. However, since the underlying undisturbed dynamical system influences the orbits during the implementation of a push the definition would be less clear-cut. We will therefore not define this, but illustrate this with so-called Poincaré sections and maps. This method comes down to constructing a discrete map by means of intersections of an orbit, our flow-push/kick

trajectory, with a hyperplane. The hyperplane or Poincaré section is chosen such that the orbit passes through the plane after a certain time and returns to this hyperplane as well. If the distance between the consecutive points given by the map decreases to zero if time continues this is a strong indication that the orbit is indeed periodic [10]. How these Poincaré sections and maps exactly work, can be found in Section 6.3. Figure 5.5 shows us that the distances between the consecutive points in the used Poincaré section, $S_{\text{lin}} = \{(x, y) \in \mathbb{R}^2 : x = 0, y > 0\}$, indeed decrease logarithmically for linear system (5.1). Thus, the flow-push trajectory converges to a periodic orbit. Note that this logarithmic relation does not hold at the very beginning of the flow-push map, the flow-kick orbit needs some time to converge to a periodic one. This is also the case in Figure 5.6. In Figure 5.6 the Poincaré technique is applied to the flow-push trajectories obtained on nonlinear undisturbed dynamics for different push times for a section given by $S_{\text{nonlin}} = \{y = -0.4, x \geq 1.25\}$, the nonlinear dynamics from the figure are given by

$$\begin{cases} \dot{x} = -x - y, \\ \dot{y} = \frac{1}{5}x + \frac{1}{2}y - x^2 y \end{cases} . \tag{5.2}$$

Some flow-push trajectories for (5.2) are depicted in Figure 5.7. In addition, some flow-push trajectories defined on (5.1) are displayed in Figure 5.4.

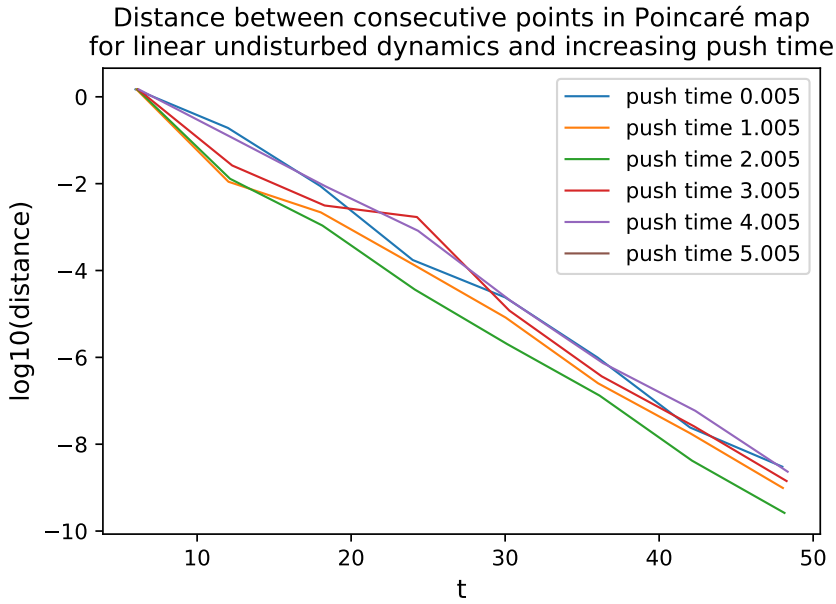

Figure 5.5: Distance between consecutive points in Poincaré map for flow-push trajectories defined by $(\tau, \tau_p, \kappa) = (6, \tau_p, (-1, 1))$ ***initiated at*** $(0.0502..., -0.0016...)$ ***for increasing push time,*** τ_p***, on undisturbed dynamics given by*** (5.2)***.***

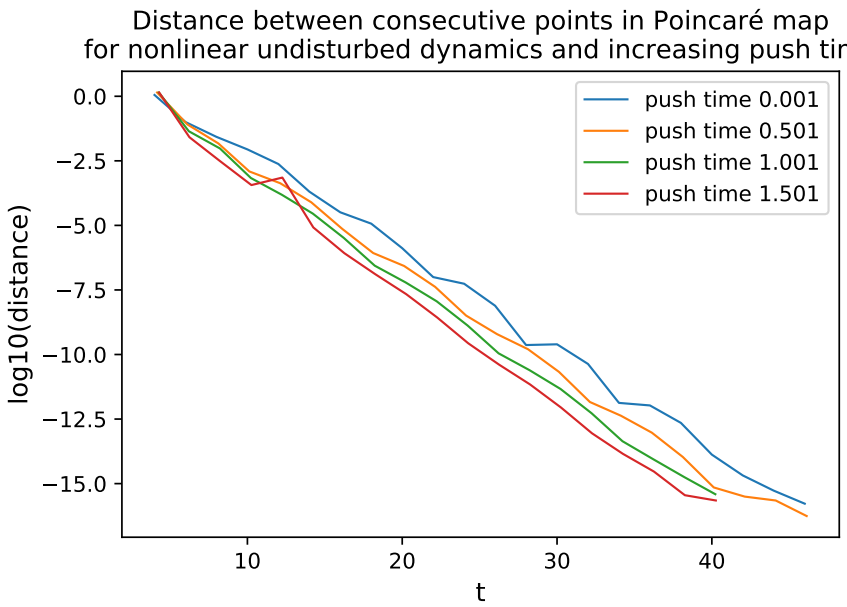

Figure 5.6: ***Distance between consecutive points in Poincaré map for flow-push trajectories defined by*** $(\tau, \tau_p, \kappa) = (2, \tau_p, (1.5, -1.5))$ ***for increasing push time,*** τ_p***, with flow-push trajectories initiated at*** $(0.938..., -0.476...)$ ***on the undisturbed nonlinear dynamics given by*** (5.2)***.***

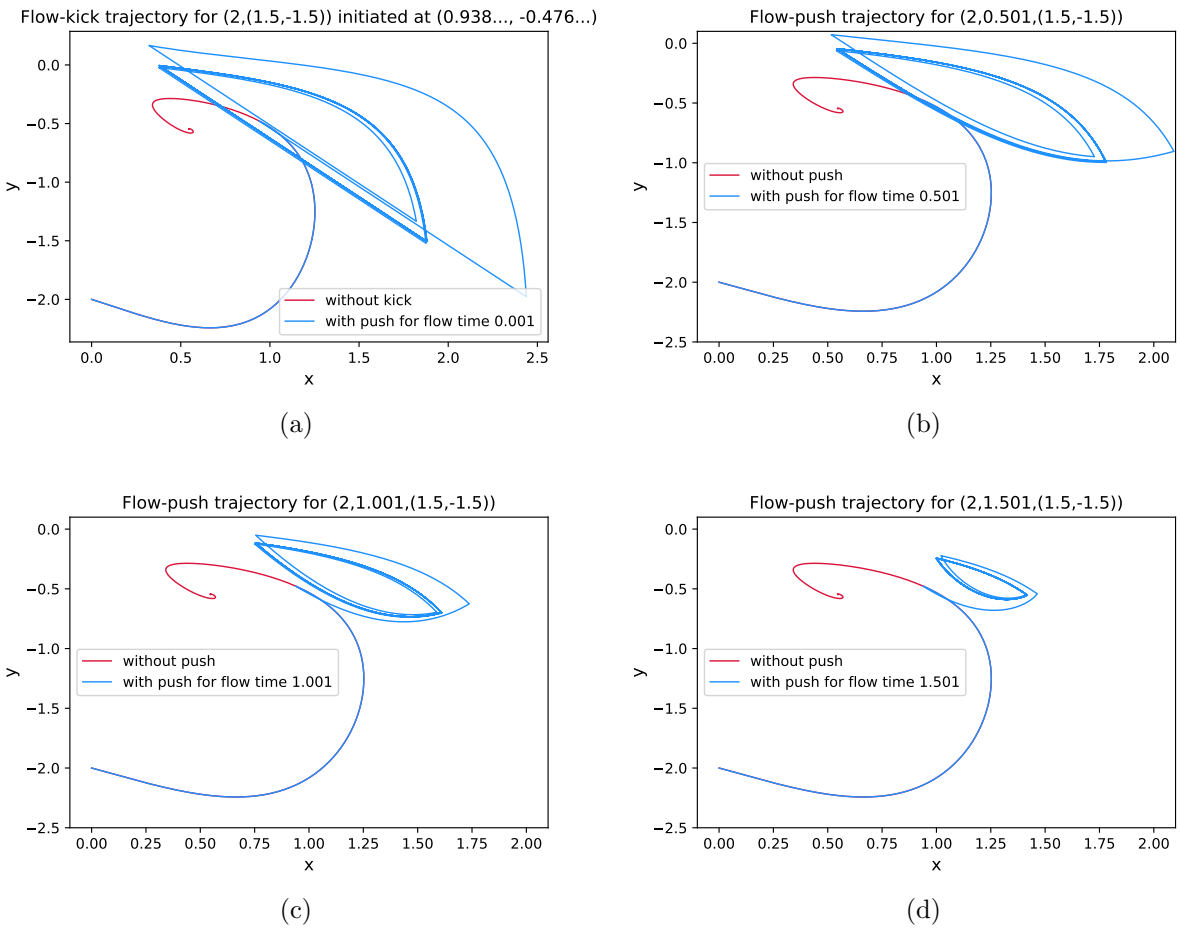

(a) (b) (c) (d)

Figure 5.7: ***Flow-push trajectories defined by*** $(\tau, \tau_p, \kappa) = (2, \tau_p, (1.5, -1.5))$ ***for increasing push time initiated at*** $(0.938..., -0.476...)$ ***on the undisturbed nonlinear dynamics given by*** (5.2)***.***

6 Fast-slow systems

Kicks and pushes are fast changes to systems of differential equations. The variables $x_1, \ldots, x_n$ in the undisturbed system function on a the time scale described by t, which is in comparison to the rapidity of the kicks and pushes much slower. This makes us wonder whether systems in which variables operate on separate time scales can be linked to flow-kick or -push systems.

This chapter will therefore first define fast-slow systems in Section 6.1. Based on this theoretical portrait an example of fast-slow systems, the three-dimensional Saltzman-Maasch climate model, is considered in Section 6.2 and 6.3.

6.1 Definition

The following definition is strongly based on the definition of fast-slow systems in [8].

Definition 6.1. *A (m,n)-fast-slow system is a system of ordinary differential equations taking the form*

$$\begin{aligned} \frac{dx}{dt} &= \dot{x} = f(x,y,\varepsilon), \\ \varepsilon\frac{dy}{dt} &= \varepsilon\dot{y} = g(x,y,\varepsilon), \end{aligned} \tag{6.1}$$

with $f : \mathbb{R}^m \times \mathbb{R}^n \times \mathbb{R} \to \mathbb{R}^m$, $g : \mathbb{R}^m \times \mathbb{R}^n \times \mathbb{R} \to \mathbb{R}^n$ and $0 < \varepsilon \ll 1$. The x-variables are called the slow variables and the y-variables the fast variables. The system can be rewritten when setting $t' = \frac{t}{\varepsilon}$, this gives the equivalent form

$$\begin{aligned} \frac{dx}{dt'} &= x' = \varepsilon f(x,y,\varepsilon) \\ \frac{dy}{dt'} &= y' = g(x,y,\varepsilon), \end{aligned} \tag{6.2}$$

We refer to t as the fast time scale and to t' as the slow time scale.

Notation for fast-slow systems has not been uniform and different conventions has been used throughout several scientific publications. Sometimes, the naming of the slow and fast variables has been interchanged or are f and g not separated explicitly stated [8]. In Figure 6.1 the phase plane of the so-called Van der Pol equation given by

$$f(x) = \begin{cases} \dot{x} &= y \\ \varepsilon\dot{y} &= (1-x^2)y - x \end{cases}, \tag{6.3}$$

is depicted [8]. In line with the nonuniform tradition of notation in fast-slow systems research, the used notation in the definition of the Van der Pol equation differs from Definition 6.1. In this case, f is not only describing the slow variables of the system, but both slow and fast variables. This will occurs more often in the next section, since this is more convenient for low-dimensional systems. The Van der Pol equation was introduced by Balthasar van der Pol in 1920 and is known as a type of limit cycles in electrical circuits that use vacuum tubes. To prove that the system has a limit cycle, Liénard's theorem is used and therefore, the transformed version of the system enjoys greater fame than the version stated in (6.3) [8]. When comparing the phase space of the Van der Pol equation to Figure 6.2, it looks as if a push can be defined on non-fast-slow system such that the limit cycles match in some way. Chapter 8 embroiders a little on this observation, since it might be worthwhile examining thoroughly.

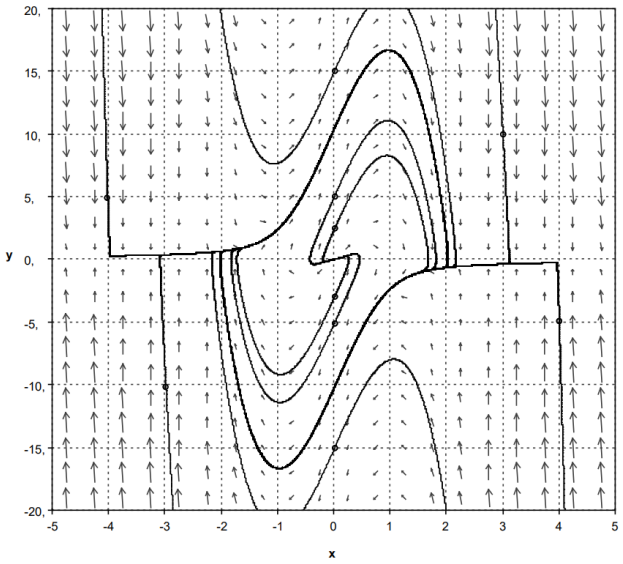

Figure 6.1: Phase plan of vector field defining Van der Pol equation for $\varepsilon = \frac{1}{10}$ with some highlighted orbits.

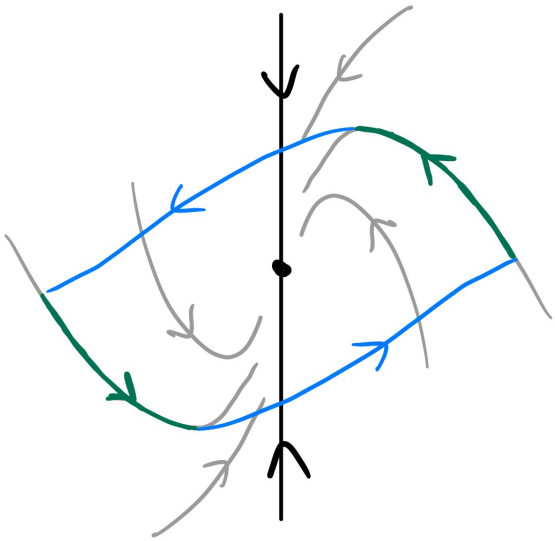

Figure 6.2: Flow-push system for stable node such that periodic orbit corresponds in some way with limit cycle in Van der Pol equation from Figure 6.1.

6.2 Saltzman-Maasch model

The Saltzman-Maasch model is a conceptual model given by a 3-dimensional dynamical system and describes the relation between the global ice mass, x, the concentration of atmospheric carbon dioxide, y, and the volume of the North Atlantic Deep Water (NADW) production, z, theoretically [4]. The conceptuality of the Saltzman-Maasch model is about the fact that the derivation of the model involves physical arguments, but that it is not guaranteed that it actually corresponds to what happened during the Pleistocence, see Figure 6.3.

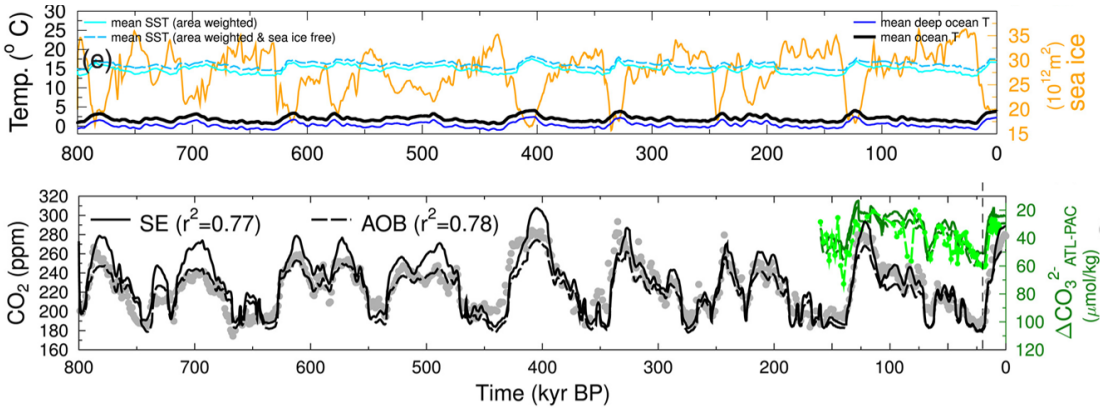

Figure 6.3: Atmospheric CO_2 concentration in black and green and total global ice mass during the Pleistocene in yellow [9].

Due to the fact that the rapid evolution of the NADW production occurs in a short time, while the global ice mass and the concentration of atmospheric carbon dioxide change on slow time scales, one can easily conclude that the Saltzman-Maasch model is a fast-slow system [3]. The model is given by the following dynamical system:

$$\begin{aligned} \dot{x} &= -x - y, \\ \dot{y} &= ry - pz + sz^2 - yz^2 \\ \dot{z} &= -qx - qz. \end{aligned} \tag{6.4}$$

Note that we need various transformations to obtain the real, positive coefficients p, q, r and s to formulate the model in an exact way. Hence, the correspondence of x to the global ice mass, of y to the atmospheric CO_2 concentration and z to the NADW production is not immediate. More details on these transformations and the rest of the derivation of the model can be found in [4]. The effective ratio of the characteristic time scales of the change in global ice mass and the NADW production is given by the coefficient $q > 1$. The coefficients p and r represent the rates at which the CO_2 concentration and the volume of the NADW changes, respectively. The model is symmetric if $s = 0$. Although it is not realistic that this is the case, since glacation and deglacation do not occur at the same rate, we assume for the convenience that it is.

As carbon dioxide is a greenhouse gas, a high concentration leads to global temperature rise, which will eventually result in a smaller global ice mass. This gives that the change in ice mass, x, depends on the atmospheric CO_2 concentration, y.

The atmospheric CO_2 concentration also influences the volume of the NADW production, z. The NADW is a deep water mass formed in the North Atlantic Ocean and plays an important role in the thermohaline circulation. This circulation is part of the large-scale ocean circulation from the southern hemisphere into the North Atlantic that is fueled by temperature differences created by surface heat and fresh water supply. Evaporation and fusion with other water masses change the salinity of the water flowing northward. An increase in salinity and a drop in temperature makes this water flow sink when it reaches the North Atlantic. The great depths of the North Atlantic accommodate a thick layer of cold water and the outflow of this layer is the volume of the NADW production. Furthermore, the larger the NADW volume, the more atmospheric CO_2 is absorbed by the ocean, since the oceanic pump becomes stronger if this volume increases. Thus, the dependency of z on x is linear to leading order.

6.3 Periodicity in Saltzman-Maasch model approached numerically and theoretically

The processes described by the model hint to periodicity. For $\dot{y} > 0$ we have that the amount of carbon dioxide increases, if y becomes positive, this leads to a decrease in the total amount of ice, $\dot{x} < 0$. Now, x becomes smaller than 0 and since $\dot{z} = -qx - qz$, we deduce that the volume of the NADW will increase. If z becomes positive again, the amount of atmospheric CO_2 decreases and, with $\dot{y} = ry - pz + sz^2 - yz^2$, y becomes negative. Once y is negative, the opposite happens. Figures 6.4 and 6.5, plotted with `saltzmanmaasch.py` (see Appendix A.3), suggest convergence to a periodic orbit of a certain initial value in the Saltzman-Maasch model.

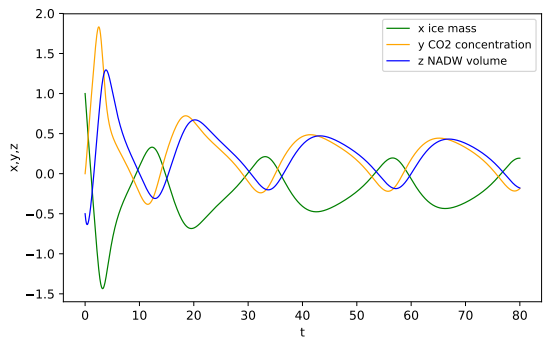

***Figure 6.4:** Periodicity in the Saltzman-Maaschmodel for $p = 0.8$, $q = 1.6$, $r = 0.6$ and $s = 0.8$ for initial value $(x, y, z) = (1, 0, -0.5)$ for x, y and z separately.*

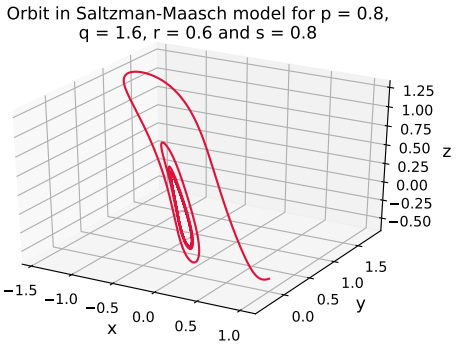

***Figure 6.5:** Convergence to periodic orbit in the Saltzman-Maaschmodel for $p = 0.8$, $q = 1.6$, $r = 0.6$ and $s = 0.8$ for the red trajectory of initial value $(x, y, z) = (1, 0, -0.5)$.*

This observation can be verified with Poincaré maps, which arise naturally when taking sections of the flow.

Definition 6.2. *For a flow ϕ_t in $\mathbb{R}^n$ a section S is a smooth surface of dimension $n-1$ such that for all $x \in S$ we have that the velocity vector of $\phi_t(x)$ is not tangent to S.*

Definition 6.3. *For a section S of flow ϕ_t in $\mathbb{R}^n$, we define the Poincaré map $P : S \to S$ for $x \in S$, with return time $T(x)$ for the first return of $\phi_t(x)$ to S, by*

$$P(x) = \phi_{T(x)}(x).$$

However, it can be the case that $T(x)$ does not exist for all x in S, if $\phi_t(x)$ does never return to S, then the Poincaré map is not well-defined. The Banach fixed-point theorem on complete metric space $S \subset \mathbb{R}^n$ gives that $\{P^n(x)\}$ converges if there exists a contraction mapping on S. This is the case if the distance between consecutive points in $\{P^n(x)\}$ gets smaller from some N forward. Let $d : \mathbb{R}^n \to \mathbb{R}$ be the Euclidean distance between two points and let $N \in \mathbb{Z}_{\geq 0}$. Define $\{d_n\}_{n\geq 0}$ such that d_n is given by $d(P^n(x), P^{n+1}(x))$ and assume that for all $n \geq N$, which gives rise to a contraction mapping, and thus a periodic orbit [10].

Proposition 6.1. *If the sequence $\{P^n(x)\}$ converges to a limit point for a Poincaré map P defined for section S and flow ϕ_t, then there exists a periodic orbit for ϕ_t.*

Proof. The proof follows by definition. □

In Figure 6.6 we see the distance between consecutive points of the Poincaré map for some section and some parameter values of p, q, r and s decreases logarithmically. The distance between the values is smaller than 10^{-4} from the thirteenth return to the section on wards ($t = 133.721$). The orbit defining the Poincaré map returns to the defined section fourteen times for $t \in (0, 150)$. This gives us that the orbit of $(1, 0, -\frac{1}{2})$ converges to a periodic orbit [10]. The fact that the graph is steeper on $(0, 20)$ than for the rest of the run time, can be explained by the fact that $q > 1$ in our example. The orbits of the fast-slow system with initial value not in the critical manifold, which is given by $C_0 = \{(x, y) \in \mathbb{R}^m \times \mathbb{R}^n : f(x, y, \varepsilon) = 0\}$, thus, for $q \to \infty$, are attracted to this manifold and after some time the orbits thrive on C_0 [8].

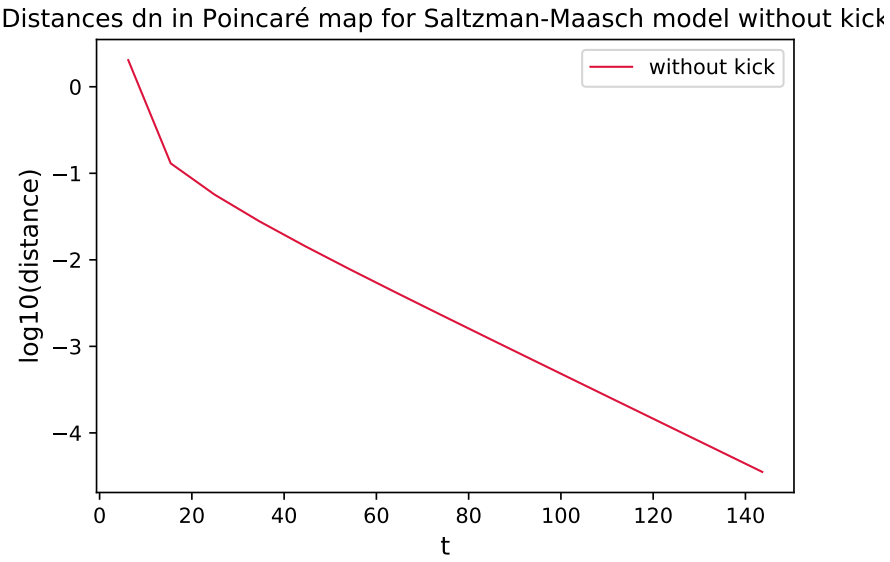

Figure 6.6: Distance between consecutive points of Poincaré map on $S = \{(x, y, z) \in \mathbb{R}^3 : z = 0$ and $x > 0\}$ in Saltzman-Maasch model with $p = 0.8, q = 1.6, r = 0.6$ and $s = 0.8$ if no kicks are applied. This figure is plotted with `saltzmanmaasch_distance.py`, see Appendix A.3.

Disturbances can, of course, also be applied to fast-slow systems such as the Saltzman-Maasch model. Consider the disturbances (τ_i, κ) with $\kappa = (0.5, 1.5, 0.5)$ for with $t_1 = 9.9$, $t_2 = 10$ and $t_3 = 10.1$. For the various flow time we obtain Figure 6.7. Due to the applied disturbances the distances d_n do now not decrease logarithmically. For the different flow times, the flow-kick trajectories behave differently, since the orbits need first to converge to a periodic orbit. The flow-kick trajectories first need to stabilize and approach the orbit for which Definition 4.2 holds and it appears that it takes therefore longer for the distances to decrease logarithmically for τ_3 in comparison to τ_1 and τ_2. The sequence $\{d_n\}_{n\geq 0}$ maps might even allow us to determine the period of the limit cycle in the Saltzman-Maasch model, see Chapter 8.

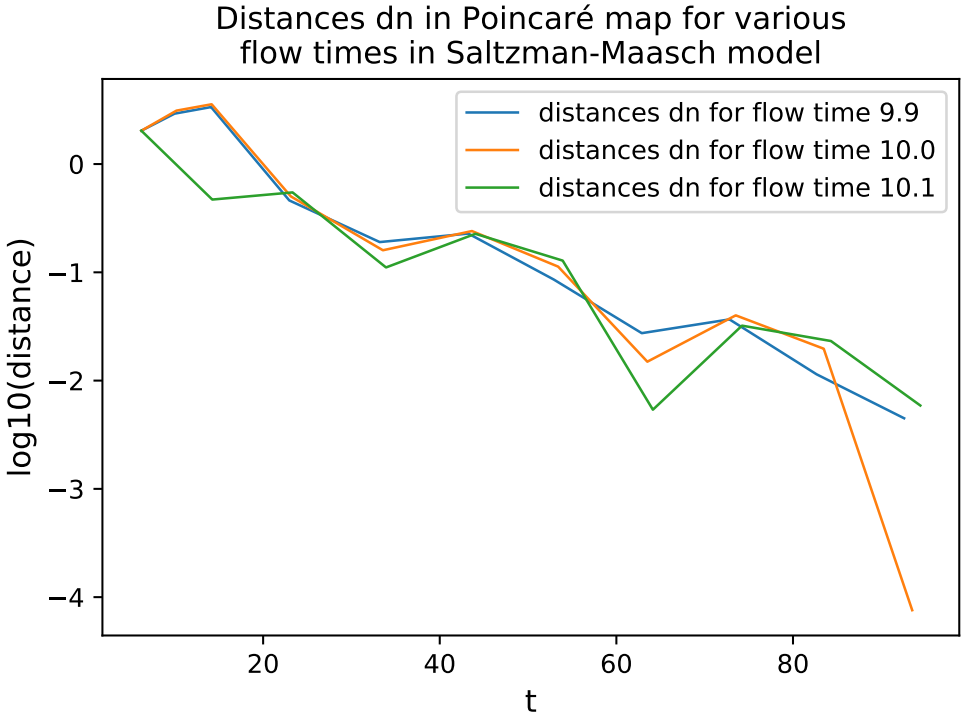

Figure 6.7: Distance between consecutive points in Poincaré map do not decrease the same for different flow times.

7 Conclusion

Flow-kick dynamical systems can be a useful tool in scientific research regarding a great range of issues. Repeated human influences or natural disturbances can be taken into consideration and be incorporated into the mathematical analysis of these systems with an increasing degree of complexity for the number of variables for which it is defined.

This increasing complexity is exemplified by the resilience boundaries discussed in Chapter 3 on one-dimensional flow-kick systems and the resilience surfaces established in Chapter 4. Not assuming that the vector field defining the underlying, undisturbed dynamics of the flow-kick system has only one local minimum on a certain interval contained in the basin of attraction of asymptotically stable equilibrium, leads to the observation, that the basin of attraction can be divided into *at least* two intervals for disturbance (τ, κ) such that the flow-kick trajectory converges to a different convergence interval when initiated in these distinct initial condition intervals, I_r from Definition 3.5.

When the kick magnitude is interfered with after some time T, a flow-kick trajectory is re-initiated and therefore it might be the case that an adjustment steers the orbit away from collapse or towards a different convergence interval. The break down of a fish population in a lake disturbed by overfishing can this way be conquered by increasing the flow time or decreasing the kick size when the flow-kick trajectory is not yet kicked out of the basin of attraction, in particular, below the Allee threshold of the considered system describing the fish population size. In classifying the intervals in which the flow-kick trajectory is initiated the disturbance has a leading role, instead of the initial value, which is determining for the resilience boundary.

The resilience boundary is expanded to higher-dimensional systems in Chapter 4. We see that the direction and length of the kick can have great influence on whether or not a disturbance is stable or unstable. If there is a point $\tilde{x}$ in the phase space of the system such that flowing forward for the recovery time after applying kick κ to this point leads to the same position of the flow-kick trajectory in the orbit as before the disturbance happened, so $\phi_\tau(\tilde{x} + \kappa) = \tilde{x}$. Therefore, a flow-kick trajectory converges to a periodic orbit inside of the basin of attraction of an asymptotically stable equilibrium. It is clear that the undisturbed dynamics of the system plays a decisive role. However, for unstable and stable but not asymptotically stable equilibria, this is not by definition the case. A periodic orbit can artificially be created by applying a disturbance with very high precision, but the characters of the solutions do not automatically lead to convergence to the periodic orbit, even though one would apply the first disturbances in a small neighborhood of $\tilde{x}$. For asymptotically stable equilibria it is nonetheless possible for every recovery time τ to find a kick κ such that the flow-kick trajectory of an equilibrium stays in a neighborhood of the equilibrium after some time $T \geq 0$.

Since it is sometimes not realistic that kicks are instant, flow-push systems are considered. It appears, however, that homogeneous pushes do not differ a lot from instant kicks, especially pushes for which the push time is equal to the flow time, so that the system has zero time to recover from the push. The flow-push system is in this case comparable with an undisturbed dynamical system, which is based on the original undisturbed dynamics. Poincaré sections illustrate how long it takes for a flow-push trajectory to become periodic. The push time influences this process in the beginning, but after some time in a linear system all orbits converge almost as fast to a periodic orbit. In nonlinear systems, it can be the case that the flow-push orbit converges a lot faster to this periodic orbit than for others. Thus, the underlying system is again crucial.

Chapter 6 deals with fast-slow systems and considers the Saltzman-Maasch model as an example. The fast-slow systems were introduced because of a possible link with flow-push dynamics. However, this link appeared less evident than expected, see Chapter 8, and more time is needed to investigate it in detail. Nonetheless, disturbances were applied to the Saltzman-

Maasch model and by means of Poincaré sections it was made clear that the flow-kick orbit converges to a periodic orbit. The rate at which the orbits converge to this periodic orbit depends on the flow-time.

Altogether, the framework of flow-kick dynamical systems shows a great variety in possible approaches. It appears that the undisturbed dynamical system and the applied disturbance are closely connected. The subdivision of the phase space of (2.1) in the different basin of attractions for the determines the disturbances to which the system is resilient. Besides, subdivisions of the basin of attraction also disclose properties of flow-kick trajectories that converge to a certain periodic orbit. In what way the flow-kick techniques are promising will be described in the following chapter.

8 Discussion

So far, this thesis discussed flow-kick dynamics in one-dimensional and two-dimensional systems, we expanded the theoretical framework of flow-kick dynamics by looking at non-instant kicks, pushes with a certain duration, and fast-slow systems were considered. Exploring these subjects led to some interesting observations and also broached new aspects of the theory. Unfortunately, we could not gain more in-depth knowledge on these new perspectives due to the time limit of this project. Next to some clarifications on recommendations already made in previous chapters, the current chapter provides a reflection on the done research.

Chapter 3 considers flow-kick maps on one-dimensional undisturbed dynamical systems and zooms in on resilience boundaries, convergence intervals and disturbances $(\tau, K(t))$ for which the kick $K(t)$ depends on how much time has passed. The definition of resilience boundaries for flow-kick trajectories of asymptotically stable equilibria is extended to resilience boundaries for flow-kick trajectories that are initiated at a point different from equilibrium, a, in the basin of attraction of the equilibrium a, $\mathcal{B}(a)$. The geometrical representation of this resilience boundary (or actually surface) should be investigated in further depth. In other words, the properties of the image of $A : \mathcal{B}(a) \times \mathbb{R}_{>0} \to \mathbb{R}_{>0}$ given by $\bigcup_{x_0 \in \mathcal{B}(a)} \{A(x_0, \kappa) = \tau : \kappa > 0\}$ should be considered more extensively. The maximal kick $\kappa_{\max}$ that can be applied to $x_0 \in \mathcal{B}(a)$ for which the flow-kick trajectory is stays in $\mathcal{B}(a)$ or is not immediately kicked out of $\mathcal{B}(a)$ when the first kick is applied, depends on the distance between this point and the boundary of the basin of attraction, $d(x_0, \partial\mathcal{B}(a))$. This way, adding an extra axis to the (τ, κ)-space, see Figure 3.2, representing the values x_0 at which the flow-kick trajectories begins, results in a surface in a three-dimensional "disturbance" space. Properties of the resilience surface in this space can be determined with the fact that vector field $f \in C^1$ dictating the undisturbed dynamics can have several local minima on $\mathcal{B}(a)$ in mind. We expect the several extrema of f to result in anomalies in the smoothness of the obtained surface, since the basin of attraction can be split up in intervals for which the initial values can have different convergence intervals. For this subdivision of the basin of attraction of a is determined by the applied disturbance, this must also be taken into consideration. To conclude the effects on the surface, however, these basic properties should first be ascertained for vector fields with only one minimum on $\mathcal{B}(a)$. Is this surface for example convex for f with one minimum and is this convexity compromised when f has several?

In addition, studying the consequences of disturbances for which the kick is dependent on time might be worthwhile, since the outcome of changing a kick based on an observation can have tremendous impact on the direction in which a system is headed. Reducing or adjusting kicks can make models more realistic. Beach nourishment could be a great example for this, since erosion of the coastal line of defence depends on a lot of factors and adjusting the quantity of sand replenishment is not uncommon [6].

As suggested in Chapter 4 the resilience surfaces can not be depicted as easily for higher-dimensional systems as for one-dimensional systems. The direction of kick κ add to this complexity directly. Besides this, it might be interesting for further research to pursue the influence of the character of an equilibrium at which a flow-kick trajectory is initiated on the resilient and non-resilient set, which is already illustrated in Section 4.2, but can be analyzed more extensively. For example, by some numerical analysis and zooming in on the possibility of creating a periodic orbit for stable centers via a disturbance (τ, κ) such that the flow-kick trajectory passed through the center point and stays there for flow time half of the period of the orbits around the center, x_*. This way, the periodic flow-kick orbit can be mapped to a semicircle in a neighborhood of this equilibrium.

However, when κ would not exactly be the vector between the initial value of the flow-kick trajectory and another point in the orbit of this x_0 in this neighborhood for a certain flow time

τ, the disturbance (τ, κ) generates a periodic orbit consisting of two orbits that can be mapped to two semicircle orbits with different radii which can be found when linearizing the system in a neighborhood of x_*. One radius is in this linear system r, the radius of the orbit of x_0 after mapping it to the linearization and the radius of the newly obtained semicircle $r \pm h(|\kappa|))$ connected by the straight kicks. Periodic flow-kick orbits now consist of multiple disturbances and in this way recovering from disturbances around stable equilibria (see Definition 4.2) should be reformulated again based on the character of the equilibria. This observation should be worked out and, of course, proved in detail.

In Section 4.3 was proved that the flow-kick trajectory of an asymptotically stable equilibrium, x_*, stays in the neighborhood of this equilibrium for a kick with given flow time. A main aspect in the proof was the utilization of Theorem 2.1. However, Theorem 2.1 does not hold on the whole of the basin of attraction of x_*, $\mathcal{B}(x_*)$. Further research should determine the resilience boundary of all flow-kick trajectories initiated in $\mathcal{B}(x_*)$, just as in Proposition 3.1.

Next to instant disturbances, this thesis discussed so-called flow-push dynamics in Chapter 5. The assumption that these pushes are applied homogeneously, can in addition be loosened a bit and this might open up the possibility to link the theoretical framework of flow-push dynamics to real-life examples of disturbances. As it happens, disturbances in real-life systems can also be build up from zero instead of being instantly "switched on", which occurs when the push has the same value during the whole push time. Consider for example the rising average temperature in the ocean which lead to massive coral bleaching and more absorption of CO_2 into the oceans such that the acidity rises. The slow increase of the temperature can be considered as a slow push [2]. In Section 5.1 was noted that the time the system has to recover from a kick needs to be greater than zero, by increasing the push time of a disturbance given by (τ, τ_p, κ) the difference between τ and τ_p therefore goes to zero. However, one could fix $\tau - \tau_p$ and with increasing the push time, τ would change. This might influence the rate at which a flow-push trajectory becomes periodic.

In Chapter 6 it is observed that the link between flow-kick an flow-push dynamics is promising. In flow-kick systems, the kick is approached as an external factor that influences the system. In fast-slow systems, the push or kick is an internal property. In fast-slow systems sometimes the fast dynamics determine the system and sometimes the slow has the upper hand. This is illustrated by means of the Van der Pol equation in Figure 6.1. The undisturbed Van der Pol dynamics is linked with a flow-push system in Figure 6.2 since the same limit cycle as in the Van der Pol system can be obtained by applying a push to the critical manifold C_0, with

$$C_0 = \{(x, y) \in \mathbb{R}^m \times \mathbb{R}^n : f(x, y, \varepsilon) = 0\},$$

in some restricted vector field $f \in C^1$. The definition of critical manifolds yields

$$C_0 = \left\{(x, y) \in \mathbb{R}^2 : y = \frac{x}{1 - x^2} \text{ and } x \in \mathbb{R} \setminus \{\pm 1\}\right\},$$

for the Van der Pol equation and this manifold plays an important role in connecting the fast-slow systems to flow-push systems. Further research should clarify the role of the critical manifold in linking fast-slow to flow-kick or -push systems.

The Saltzman-Maasch fast-slow model described in Chapter 6, is analyzed in detail in [4] and [3]. These publications display the great complexity of the model by spelling out bifurcations and different structures that can be found in the model for $q \to \infty$, therefore, on the critical manifold of the system. Since coefficients are based on physical parameters it would be recommended to look further into what kicks or pushes would be relevant to apply and what these disturbances mean for the periodicity of the model. Moreover, we expect that the period of the limit cycle for some values of the parameters in the Saltzman-Maasch model can be found through Poincaré maps. The distances d_n between the consecutive points might decrease faster when the flow time

would be closer to the period of the limit cycle from the model. It would then namely take less time for the flow-kick trajectory to converge to a periodic orbit. This would also be applicable in other (non-fast-slow) systems such as Figures 5.3, 5.5, and 5.7, but then to determine the time it takes to return to a section for an orbit in the undisturbed dynamics, around for instance a stable focus. The sections that should be considered for Figure 5.3 until 5.5 would be the lines $y = 0$ or $x = 0$. Besides this, the numerical analysis of the Saltzman-Maasch model could have been more focussed on the fast-slow aspect of the system, by choosing a (much) greater value for q. This remark leads to the following observations about the research in general.

In the numerical analysis this thesis mainly targeted particular examples, often distinguishing linear and nonlinear dynamical systems. Further research could and should rearrange this structure by qualifying the hyperbolic equilibria by means of their characters which can be determined via their linearizations. This way a broader range of features can be compared and analyzed systematically. While adjusting this structure, one should also pay attention to bifurcation theory and constructing resilience boundaries (as curves or surfaces) by adjusting disturbances only a little. Even though the obtained numerical results could have been sharper, for instance by determining numerical and rounding errors, applying a more exact algorithm than the forword Euler method to find solutions of the undisturbed dynamics or finding intersections with Poincaré sections, we were able to answer the research questions stated in the first chapter in Chapter 7.

References

[1] M. Braun. Differential Equations and Their Applications. An Introduction to Applied Mathematics. Springer Verlag, New York, 3 edition, 1982.

[2] C. Eakin, H. Sweatman, and R. Brainard. The 2014–2017 global-scale coral bleaching event: insights and impacts. Coral reefs, 38(4):539–545, 2019.

[3] H. Engler, H. Kaper, J. Kaper, and T. Vo. Dynamical systems analysis of the Maasch–Saltzman model for glacial cycles. Physica. D, 359:1–20, 2017.

[4] Hans Engler, Hans G. Kaper, Tasso J. Kaper, and Theodore Vo. Modeling the Dynamics of Glacial Cycles. In Hans G. Kaper and Fred S. Roberts, editors, Mathematics of Planet Earth: Protecting Our Planet, Learning from the Past, Safeguarding for the Future, pages 3–33. Springer International Publishing, Cham, 2019.

[5] J. Garnier, L. Roques, and F. Hamel. Success rate of a biological invasion in terms of the spatial distribution of the founding population. Bulletin of Mathematical Biology, 74(2):453–473, 2012.

[6] H. Hanson, A. Brampton, M. Capobianco, H. Dette, L. Hamm, C. Laustrup, A. Lechuga, and R. Spanhoff. Beach nourishment projects, practices, and objectives—a European overview. Coastal engineering (Amsterdam), 47(2):81–111, 2002.

[7] A. Kramer, B. Dennis, A. Liebhold, and J. Drake. The evidence for Allee effects. Population ecology, 51(3):341–354, 2009.

[8] C. Kuehn. Multiple Time Scale Dynamics, volume 191 of Applied Mathematical Sciences. Springer International Publishing, Cham, 2015.

[9] P. Köhler and G. Munhoven. Late Pleistocene Carbon Cycle Revisited by Considering Solid Earth Processes. Paleoceanography and Paleoclimatology, 35(12), 2020.

[10] J. Meiss. Differential dynamical systems. Society for Industrial and Applied Mathematics, Philadephia, PA, 2007.

[11] K. Meyer, S. Iams, A. Hoyer-Leitzel, I. Klasky, V Lee, S. Ligtenberg, R. Bussmann, and M. Zeeman. Quantifying resilience to recurrent ecosystem disturbances using flow–kick dynamics. Nature Sustainability, 2018.

[12] S. Mobaied, N. Machon, A. Lalanne, and B. Riera. The Spatiotemporal Dynamics of Forest–Heathland Communities over 60 Years in Fontainebleau, France. ISPRS International Journal of Geo-Information, 4(2):957–973, 2015.

[13] L. Theunissen and History of Science. The Oostvaardersplassen Fiasco. Isis, 110(2):341–345, 2019.

[14] E. Vanguelova, S. Benham, R. Pitman, A. Moffat, M. Broadmeadow, T. Nisbet, D. Durrant, N. Barsoum, M. Wilkinson, F. Bochereau, T. Hutchings, S. Broadmeadow, P. Crow, P. Taylor, and T. Durrant Houston. Chemical fluxes in time through forest ecosystems in the UK – Soil response to pollution recovery. Environmental pollution (1987), 158(5):1857–1869, 2010.

A Python code

The used Python code is included here. One-dimensional flow-kick systems can be plotted with the code from Appendix A.1, two-dimensional with the one in Appendix A.2 and the Saltzman-Maasch model is simulated with the code from A.3. Note that the several documents can be fused to a connected project, however, one can select easily the desired functions by selecting the right document with the needed variables included.

A.1 Python code for one-dimensional flow-kick systems

A.1.1 `flowkick.py`

```
import matplotlib.pyplot as plt
import numpy as np
import scipy.integrate as integrate

N = 10000   # number of steps
T = 8   # total run time
dt = T/N
t_flow = 0.042 # flow or recovery time for flow-kick system
k = 0.25      # kick size
k_dept = -16
k_dept2 = -16
threshold_dept = 7
t_flow_dept = 1
t_flow_dept2 = 1
threshold_dept2 = 4
k_dur = 1  # length of push in time steps

x0 = 3.56 # initial value of flow-kick trajectory
X0 = 0.5
xt0 = 75

x_IV = np.linspace(2-np.sqrt(2 + np.sqrt(6)), 2+np.sqrt(2 + np.sqrt(6)), N+1)


def f(x):
    return -4*(x-2)**2 +(x-2)**4 - 2

# to find the right boundary of I
def F(x):
    return 1/f(x)

def kt(kick,time, threshold):
    if time > threshold:
        kick = kick/2
    return kick

A = 50
A_plot = np.array([])
A_plot = np.append(A_plot, A)
K = 200

def Allee(x):
    return 0.5*x*(x/A-1)*(1-x/K)

t = np.linspace(0,T,N+1)
x = np.array([])
X = np.array([]) # second initial value
```

```
xt = np.array([]) # with time dependent kick
xG = np.array([])
XG = np.array([]) # save kicks for second initial value
xGt = np.array([]) # with time dependent kick
xGt2 = np.array([]) # with time dependent kick
I = np.array([])

x = np.append(x, x0)
xG = np.append(xG, x0)
X = np.append(X, X0)
XG = np.append(XG, X0)
xt = np.append(xt, xt0)
xGt = np.append(xGt, xt0)
xGt2 = np.append(xGt2, xt0)

kicks = 1
kicks_dept = 1
kicks_dept2 = 1

for n in range(N):
    # implementation forward euler
    A_plot = np.append(A_plot, A)
    x = np.append(x, x[-1] + dt*f(x[-1]))
    X = np.append(X,X[-1] + dt*f(X[-1]))
    xt = np.append(xt,xt[-1] + dt*Allee(xt[-1]))
    xG = np.append(xG, xG[-1] + dt*f(xG[-1]))
    XG = np.append(XG,XG[-1]+dt*f(XG[-1]))
    xGt = np.append(xGt,xGt[-1] + dt*Allee(xGt[-1]))
    xGt2 = np.append(xGt2,xGt2[-1] + dt*Allee(xGt2[-1]))
    # applying kicks
    if kicks_dept == int(t[n]/t_flow_dept) and n!= 0:
        xGt[-1] += kt(k_dept, t[n], threshold_dept)
        kicks_dept += 1
        # to check at what IV the flow-kick trajectory is reinitated
        if kicks_dept2 == 7:
            print("new IV: ", xGt[-1]-0.5*k_dept)
    if kicks_dept2 == int(t[n]/t_flow_dept2) and n!= 0:
        xGt2[-1] += kt(k_dept2, t[n], threshold_dept2)
        kicks_dept2 += 1
        if kicks_dept2 == 4:
            print("new IV: ", xGt[-1]-0.5*k_dept2)
    if kicks == int(t[n]/t_flow) and n != 0:
        if kicks == 1:
            print("initial value x0:  ", xG[-1])
            print("initial value X0:  ", XG[-1])
            print("initial value xt0: ", xGt[-1])
        for i in range(k_dur) :
            if i == 0:
                xG[-1] += k/k_dur
                XG[-1] += k/k_dur
            else:
                xG = np.append(xG, xG[-1] + dt*f(xG[-1]) + k/k_dur)
                XG = np.append(XG, XG[-1] + dt*f(XG[-1]) +k/k_dur)
            n += 1
        kicks += 1

# population size cannot be smaller than zero in natural circumstances
for n in range(N):
    if xGt[n+1]< 0:
        xGt[n+1] = 0
```

```
    if xGt2[n+1] <0:
        xGt2[n+1] = 0

#calculating all intevals over which flow time occurs between equilibria
for n in range(N):
    if x_IV[n] + k <= 2+np.sqrt(2 + np.sqrt(6)) :
        I = np.append(I, integrate.quad(F,x_IV[n],x_IV[n]+k)[0])
        if (abs(integrate.quad(F,x_IV[n],x_IV[n]+k)[0]) <= t_flow and abs(
            integrate.quad(F,x_IV[n-1],x_IV[n-1]+k)[0]) > t_flow) or (abs(
            integrate.quad(F,x_IV[n],x_IV[n]+k)[0]) >= t_flow and abs(integrate.
            quad(F,x_IV[n-1],x_IV[n-1]+k)[0]) < t_flow) and n!= 0:
             print("n:  ", n)
             print("x:  ", x_IV[n])
    else:
        I = np.append(I, 98) #dummy

# time-dependent kick in plot with Allee threshold indicated
'''
plt.plot(t, xt, linewidth = 1, color = 'darkgreen')
plt.plot(t, xGt, linewidth = 1, color = 'crimson')
plt.plot(t, xGt2, linewidth =1, color = 'dodgerblue')
plt.plot(t, A_plot, linewidth = 0.75, color = 'black', linestyle = '--')
plt.title("Kick size * 0.5 after some time in Allee model", fontsize = 13)
labels = ["without kick", "unstable disturbance", "stable disturbance", "Allee
    threshold A"]
plt.legend(labels = labels)
plt.xlabel('t', fontsize = 12)
plt.ylabel('x-position', fontsize = 12)
plt.savefig('1dim_allee_samekicks_timedept2.pdf')
plt.show()

'''

#two different intial values in one plot for fixed disturbance
plt.xlabel('t', fontsize = 12)
plt.ylabel('x-position', fontsize = 12)
plt.plot(t, x, linewidth = 1, color = 'darkgreen')
plt.plot(t, X, linewidth = 1, color = 'darkblue')
plt.plot(t, xG, linewidth = 1, color = 'crimson')
plt.plot(t, XG, linewidth = 1, color = 'dodgerblue')
plt.title("Disturbance (t,k) = (0.042,0.25) on dx/dt = (x-2)^4-4(x-2)^2-2",
    fontsize = 13)
labels1 = ["without kick for x0 = 0.771...", "without kick for ~x0 = 0.265...",
    "with kick for x0 = 0.771...",  "with kick for ~x0 = 0.265..."]
plt.legend(labels=labels1,loc='center right')
plt.savefig('1dim_kick.pdf')
plt.show()

# plotting undisturbed dynamics
plt.xlabel('x', fontsize = 12)
plt.ylabel('f', fontsize = 12)
plt.title("Undisturbed dynamics for dx/dt = (x-2)^4-4(x-2)^2-2", fontsize = 13)
x_plot = np.linspace(-0.2,4.2,100)
plt.plot(x_plot,f(x_plot), linewidth = 1, color = 'darkgreen')
plt.savefig('1dim_undisturbed.pdf')
plt.show()
```

A.2 Python code for two-dimensional flow-kick systems

A.2.1 `flowpush.py`

```
import matplotlib.pyplot as plt
import numpy as np

N = 20000 # total of steps
T = 25 # total run time
dt = T/N # size of time steps
t_flow = 2 # flow time
k1 = -1 # first argument of kick
k2 = 0 # second argument of kick
k_duration = 1 # how many time steps the push lasts
k_duration_time = k_duration*dt # push duration in time and not in steps

# initial values of orbit
u0 = 0
v0 = 1

# initial values for van der pol oscillator
#u0 = -1
#v0 = 1

# coefficients for nonlinearsystem1
r = 0.5
p = 0.2

# coefficients for van der pol oscillator
#r = 10

# linearsystem1
def f1(u,v):
    return -v-u
def f2(u,v):
    return u

# nonlinearsystem1
#def f1(u,v):
#    return -u-v
#def f2(u,v):
#    return r*v+p*u-u**2*v

# nonlinearsystem2
#def f1(u,v):
#    return -u-v+np.cos(u)

#def f2(u,v):
#    return np.sin(u)

# van der pol oscillator
#def f1(u,v):
#    return v

#def f2(u,v):
#    return r*(1-u**2)*v-u

# defining time array
t = np.linspace(0,T,N+1)

#labels for plots
```

```
labels_dist = []
labels_traj = []

#while k_duration*dt <= T: # applying various pushes
if k_duration != 0: # dummy condition so that we do not have to
                    #delete all tabs when only plotting one k_duration
    kicks = True

    # defining arrays and initiating them
    dist = np.array([])
    x1 = np.array([])
    x1 = np.append(x1, u0)
    x2 = np.array([])
    x2 = np.append(x2, v0)

    xG1 = np.array([])
    xG1 = np.append(xG1, u0)
    xG2 = np.array([])
    xG2 = np.append(xG2, v0)

    for n in range(N):
        #generating orbit without push or kick
        x1 = np.append(x1, x1[-1] + dt*f1(x1[-1],x2[-1]))
        x2 = np.append(x2, x2[-1] + dt*f2(x1[-1],x2[-1]))
        xG1 = np.append(xG1, xG1[-1] + dt*f1(xG1[-1],xG2[-1]))
        xG2 = np.append(xG2, xG2[-1] + dt*f2(xG1[-1],xG2[-1]))
        #applying push
        if n % (int(t_flow/dt)) < k_duration and n >= k_duration and n!=0:
            xG1[-1] += k1/k_duration
            xG2[-1] += k2/k_duration
            if kicks == True:
                print("push is first applied at: (", xG1[-1] - k1/k_duration,
                                                    ",", xG2[-1] - k2/k_duration,
                                                    ")")
                kicks = False
    if k_duration*dt -k_duration:
        plot_traj = plt.plot(x1,x2,color='crimson', linewidth = 1)
        labels_traj.append("without push")
    label_traj = "with push for flow time {}" # CHANGE when kick_duration = 1
    labels_traj.append(label_traj.format(round(k_duration*dt,3)))
    plot_traj = plt.plot(xG1,xG2, color="dodgerblue",
                         label = label_traj.format(round(k_duration*dt,2)),
                         linewidth = 1)
    plot_traj = plt.legend(labels_traj)
    k_duration += 200

#make sure size of figure is right!
#plot_traj = plt.xlim(-0.1,2.1) # fixing x-range
#plot_traj = plt.ylim(-2.5,0.1) # fixing y-range
plot_traj = plt.xlabel("x", fontsize = 12)
plot_traj = plt.ylabel("y", fontsize = 12)
plot_dist = plt.title("Flow-push trajectory for (2,1.501,(1.5,-1.5))",
                      fontsize = 12)
plt.savefig("flowpush_nonlinearsystem1_flowtime3.pdf")
plt.show(plot_traj)


print("kick_duration: ", k_duration_time)

#plot development of coordinates against time
```

```
'''
plot2 = plt.plot(t,xG1, color='green', linewidth = 1)
plot3 = plt.plot(t,xG2, color='orange', linewidth = 1)
labels=["with kick", "without kick"]
plt.xlabel('t', fontsize=12)
plt.ylabel('x', fontsize=12)
plt.legend(labels=labels, loc='upper right')
plt.savefig("coordinatesflowkicktraj.pdf")
'''
```

A.2.2 flowpush_distance.py

```
import matplotlib.pyplot as plt
import numpy as np

N = 20000 # total of steps
T = 50 # total run time
dt = T/N # size of time steps
t_flow = 6 # flow time
k1 = 1.5 # first argument of kick
k2 = -1.5 # second argument of kick
k_duration = 2 # how many time steps the push lasts
k_duration_time = k_duration*dt # push duration in time and not in steps

# initial values of orbit
u0 = 0
v0 = -2

# initial values for van der pol oscillator
#u0 = -1
#v0 = 1

# coefficients for nonlinearsystem1
r = 0.5
p = 0.2

# coefficients for van der pol oscillator
#r = 10

# linearsystem1
def f1(u,v):
    return -v-u
def f2(u,v):
    return u

# nonlinearsystem1
#def f1(u,v):
#    return -u-v
#def f2(u,v):
#    return r*v+p*u-u**2*v

# nonlinearsystem2
#def f1(u,v):
#    return -u-v+np.cos(u)

#def f2(u,v):
#    return np.sin(u)

# van der pol oscillator
```

```
#def f1(u,v):
#    return v

#def f2(u,v):
#    return r*(1-u**2)*v-u

# defining time array
t = np.linspace(0,T,N+1)

# labels for plots
labels_dist = []
labels_traj = []

while k_duration*dt <= t_flow: # applying various pushes
#if k_duration != 0: # dummy condition so that we do not have to
                     #delete all tabs when only plotting one k_duration
    kicks = 1 # kick counter

    # defining arrays and initiating them
    dist = np.array([])
    x1 = np.array([])
    x1 = np.append(x1, u0)
    x2 = np.array([])
    x2 = np.append(x2, v0)

    xG1 = np.array([])
    xG1 = np.append(xG1, u0)
    xG2 = np.array([])
    xG2 = np.append(xG2, v0)

    # arrays for storing Poincar  sections
    section1 = np.array([])
    section1 = np.append(section1, 1)
    section2 = np.array([])
    section2 = np.append(section2, 1)
    t_dist = np.array([])

    for n in range(N):
        # generating orbit without push or kick
        x1 = np.append(x1, x1[-1] + dt*f1(x1[-1],x2[-1]))
        x2 = np.append(x2, x2[-1] + dt*f2(x1[-1],x2[-1]))
        # generating orbit with push or kick
        xG1 = np.append(xG1, xG1[-1] + dt*f1(xG1[-1],xG2[-1]))
        xG2 = np.append(xG2, xG2[-1] + dt*f2(xG1[-1],xG2[-1]))
        # applying push or kick
        if n % (int(t_flow/dt)) < k_duration and n >= k_duration and n!=0:
            xG1[-1] += k1/k_duration
            xG2[-1] += k2/k_duration
    #check if going through section
    for n in range(N):
        # linearsystem1
        if xG1[n] < 0 and xG1[n+1] >= 0:
        # nonlinearsystem1
        #if xG2[n] > -0.4 and xG2[n+1] <= -0.4:
        # nonlinearsystem2
        #if xG1[n] < 0 and xG1[n+1] >= 0:
            A = abs(xG2[n])/(abs(xG2[n])+abs(xG2[n+1])) # xG2 might need to be
                                                        # changed into a xG1
                                                        # for different systems
            section1 = np.append(section1, xG1[n]+A*(xG1[n+1]-xG1[n]))
```

```
            section2 = np.append(section2, xG2[n]+A*(xG2[n+1]-xG2[n]))
            t_dist = np.append(t_dist, t[n])
            dist = np.append(dist, np.sqrt((section1[-1]-section1[-2])**2
                                           +(section2[-1]-section2[-2])**2))
    # fixing stuff for plot
    label_dist = "push time {}"
    labels_dist.append(label_dist.format(round(k_duration*dt,3)))
    plot_dist = plt.plot(t_dist, np.log10(dist), linewidth = 1)
    plot_dist = plt.legend(labels_dist)
    k_duration += 400 # increasing push duration
# more stuff for plot
plot_dist = plt.xlabel("t", fontsize = 12)
plot_dist = plt.ylabel("log10(distance)", fontsize = 12)
plot_dist = plt.title("Distance between consecutive points in Poincar  map\nfor
    linear undisturbed dynamics and increasing push time",
                      fontsize = 12)
plt.savefig("dist_linearsystem1.pdf")
plt.show(plot_dist)
```

A.3 Python code for Saltzman-Maasch model

A.3.1 saltzmanmaasch.py

```
import matplotlib.pyplot as plt
import numpy as np
from mpl_toolkits import mplot3d

N = 100000 # total of steps
T = 150 #total run time
dt = T/N # size of time steps
t_flow = 10.00 #flow time

# directions of kick
k1 = 0
k2 = 0
k3 = 0

# initial
x0 = 1
y0 = 0
z0 = -0.5

# parameters Saltzman-Maasch
p = 0.8
q = 1.6
r = 0.6
s = 0.8

# coordinate functions of Saltzman-Maasch model
def f1(x,y,z):
    return -x-y

def f2(x,y,z):
    return r*y-p*z+s*z**2-y*z**2

def f3(x,y,z):
    return -q*x-q*z

# defining arrays to store values of trajectories
```

```
t = np.linspace(0,T,N+1)
x1 = np.array([])
x2 = np.array([])
x3 = np.array([])

xG1 = np.array([])
xG2 = np.array([])
xG3 = np.array([])

x1 = np.append(x1, x0)
x2 = np.append(x2, y0)
x3 = np.append(x3, z0)

xG1 = np.append(xG1, x0)
xG2 = np.append(xG2, y0)
xG3 = np.append(xG3, z0)

kicks = 1
for n in range(N):
    #first argument
    x1 =  np.append(x1,  x1[-1]  + dt*f1(x1[-1],x2[-1],x3[-1]))
    xG1 = np.append(xG1, xG1[-1] + dt*f1(xG1[-1],xG2[-1],xG3[-1]))
    #second argument
    x2 = np.append(x2, x2[-1] + dt*f2(x1[-1],x2[-1],x3[-1]))
    xG2 = np.append(xG2, xG2[-1] + dt*f2(xG1[-1],xG2[-1],xG3[-1]))
    #third argument
    x3 = np.append(x3, x3[-1] + dt*f3(x1[-1],x2[-1],x3[-1]))
    xG3 = np.append(xG3, xG3[-1] + dt*f3(xG1[-1],xG2[-1],xG3[-1]))
    if kicks == int(t[n]/t_flow) and n!= 0:
        xG1[-1] += k1
        xG2[-1] += k2
        xG3[-1] += k3
        kicks += 1
        #print("bezig", n) #useful when you are impatient
# for 3D plot
ax = plt.axes(projection='3d')
plot3D = ax.plot3D(xG1, xG2, xG3, 'crimson')
ax.set_title("Orbit in Saltzman-Maasch model for p = 0.8,\nq = 1.6, r = 0.6 and
    s = 0.8, flow time = 10",
             fontsize=12)
ax.set_xlabel('x', fontsize=12)
ax.set_ylabel('y', fontsize=12)
ax.set_zlabel('z', fontsize=12)
plt.savefig('periodicitySaMa_10.pdf')
plt.show(plot3D)

# x,y,z plotted against time
plot1 = plt.plot(t,xG1, color='green', linewidth = 1)
plot2 = plt.plot(t,xG2, color='orange', linewidth = 1)
plot3 = plt.plot(t,xG3, color='blue', linewidth =1)
labels=["x ice mass", "y CO2 concentration", "z NADW volume"]
plt.xlabel('t', fontsize = 12)
plt.ylabel('x,y,z', fontsize = 12)
plt.legend(labels=labels, loc='upper right')
plt.savefig('SaMa_variables_separately.pdf')
plt.show(plot1)
plt.show(plot2)
plt.show(plot3)
```

A.3.2 saltzmanmaasch_distance.py

```
import matplotlib.pyplot as plt
import numpy as np

N = 200000 # total of steps
T = 100 # total run time
dt = T/N # size of time steps
t_flow = 10.1 # flow time

# directions of kick
k1 = 0.5
k2 = 1.5
k3 = 0.5

#initial value
x0 = 1
y0 = 0
z0 = -0.5

# parameters Saltzmann-Maasch
p = 0.8
q = 1.6 # if q >> 1 then applying kick in slow direction does
        # not do much in the x and y direction
r = 0.6
s = 0

# coordinate functions of Saltzman-Maasch model
def f1(x,y,z):
    return -x-y

def f2(x,y,z):
    return r*y-p*z+s*z**2-y*z**2

def f3(x,y,z):
    return -q*x-q*z

# label for plot
labels_dist = []

kicks = 1
while t_flow < 10.2: # plotting for flow times 9.995, 10 and 10.005
    t = np.linspace(0,T,N+1) #time axis
    # for undisturbed dynamics
    x1 = np.array([])
    x2 = np.array([])
    x3 = np.array([])
    x1 = np.append(x1, x0)
    x2 = np.append(x2, y0)
    x3 = np.append(x3, z0)

    # for flow-kick dynamics
    xG1 = np.array([])
    xG2 = np.array([])
    xG3 = np.array([])
    xG1 = np.append(xG1, x0)
    xG2 = np.append(xG2, y0)
    xG3 = np.append(xG3, z0)

    # for Poincar  section
```

```
    section1 = np.array([])
    section1 = np.append(section1, 1)
    section2 = np.array([])
    section2 = np.append(section2, 1)

    # for dn's defined by Poincar  section
    t_dist = np.array([])
    dist = np.array([])
    kicks = 1 # kick counter

    # constructing of undisturbed dynamics and orbit influenced by disturbance
    for n in range(N):
        #first argument
        x1 =  np.append(x1,  x1[-1]  + dt*f1(x1[-1],x2[-1],x3[-1]))
        xG1 = np.append(xG1, xG1[-1] + dt*f1(xG1[-1],xG2[-1],xG3[-1]))
        #second argument
        x2 = np.append(x2, x2[-1] + dt*f2(x1[-1],x2[-1],x3[-1]))
        xG2 = np.append(xG2, xG2[-1] + dt*f2(xG1[-1],xG2[-1],xG3[-1]))
        #third argument
        x3 = np.append(x3, x3[-1] + dt*f3(x1[-1],x2[-1],x3[-1]))
        xG3 = np.append(xG3, xG3[-1] + dt*f3(xG1[-1],xG2[-1],xG3[-1]))
        if kicks == int(t[n]/t_flow) and n!= 0:
            xG1[-1] += k1
            xG2[-1] += k2
            xG3[-1] += k3
            kicks += 1
            #print("bezig: ", n) # useful when you are impatient
    # constructing intersections with section (defined in if-statement)
    for n in range(N):
        if xG3[n] > 0 and xG3[n+1] <= 0 and xG1[n] > 0:
            A = abs(xG3[n])/(abs(xG3[n])+abs(xG3[n+1]))
            section1 = np.append(section1, xG1[n]+A*(xG1[n+1]-xG1[n]))
            section2 = np.append(section2, xG2[n] + A*(xG2[n+1]-xG2[n]))
            t_dist = np.append(t_dist, t[n])
            dist = np.append(dist, np.sqrt((section1[-1]-section1[-2])**2
                                           +(section2[-1]-section2[-2])**2))
    label_dist= "distances dn for flow time {}"
    #label_dist = "without kick"
    plot_dist = plt.plot(t_dist, np.log10(dist), linewidth = 1,
                         label = label_dist.format(t_flow))
    plot_dist = plt.legend(labels_dist)
    print(dist)
    t_flow += 0.1 # increasing flow time with small steps
# making a nice plot
plt.xlabel('t', fontsize = 12)
plt.ylabel('log10(distance)', fontsize = 12)
plt.legend()
#plt.title("Distances dn in Poincar  map for Saltzman-Maasch model without kick
    ", fontsize =12)
plt.title("Distances dn in Poincar  map for various\nflow times in Saltzman-
    Maasch model",
          fontsize=12)
plt.savefig('periodicitySaMa_dist.pdf')
plt.show(plot_dist)
print(dist)
```